

---

1 Responses to Reviewer:

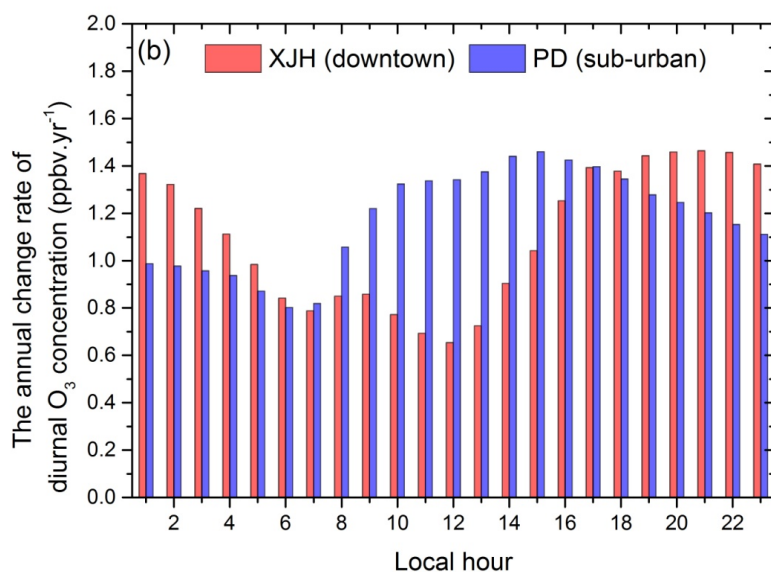
2

3 We thank the reviewer for the careful reading of the manuscript and  
4 helpful comments. We have revised the manuscript following the  
5 suggestions.

6

7 **(1) I nearly suggested major revision, because caption of Fig. 6 is**  
8 **confusing. I thought Fig. 6 is mean diurnal variation of O<sub>3</sub> and**  
9 **wondered how come nighttime O<sub>3</sub> is higher than daytime O<sub>3</sub> in XJH.**  
10 **Please clarify.**

11 Thanks for pointing out the typo of the figure caption. We have  
12 corrected the caption of Fig.6b. The Y-axis is the annual change rate of  
13 the diurnal O<sub>3</sub> concentration from 2006 to 2015 instead of O<sub>3</sub>  
14 concentration. Thus the unit in Fig. 6a is not ppbv, but ppbv.yr<sup>-1</sup>,  
15 representing the change rate of mean diurnal O<sub>3</sub> concentration from  
16 2006 to 2015.



17

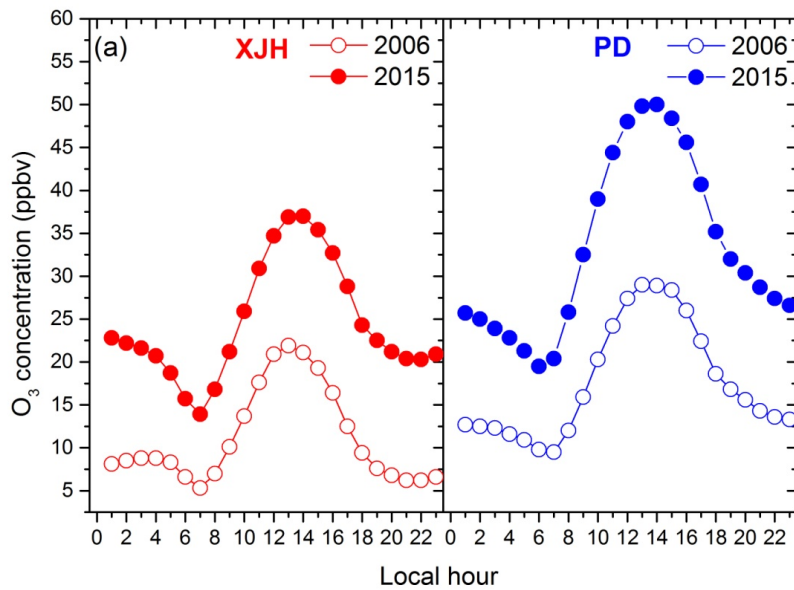
18 **Figure 6.** (b) The annual change rate of diurnal O<sub>3</sub> concentration  
 19 (ppbv.yr<sup>-1</sup>) from 2006 to 2015 at downtown site XJH (red bars) and  
 20 sub-urban site PD (blue bars).

21

22 **(2) Could you please actually present mean diurnal variations of O<sub>3</sub> in**  
 23 **2006 and 2015 in Fig. 6 ?**

24 Thanks the suggestion. To address the comments of the reviewer, we add  
 25 the additional figure to describe the mean diurnal variations of O<sub>3</sub>  
 26 concentration in 2006 and 2015 at XJH and PD site in Fig. 6a. It was  
 27 showed that the maximum and minimum O<sub>3</sub> concentrations occur in the  
 28 afternoon (14-15 pm) and in the early morning (6-7 am), respectively, at  
 29 both sites. In addition, the diurnal O<sub>3</sub> concentrations at XJH and PD all  
 30 increase significantly from 2006 to 2015. For example, the peak O<sub>3</sub>  
 31 concentration at XJH increases from 21 ppbv to 37 ppbv, meanwhile the

32 minimum O<sub>3</sub> concentration rises from 5 ppbv to 14 ppbv exhibiting  
33 higher increasing rate. Similar O<sub>3</sub> enhancement is also observed at PD  
34 site during the same period. The description has been included in the  
35 revised version.



36  
37 **Figure 6.** (a) The mean diurnal variation of O<sub>3</sub> concentration (ppbv)  
38 compared between 2006 and 2015 in XJH (red dots) and PD (blue dots).

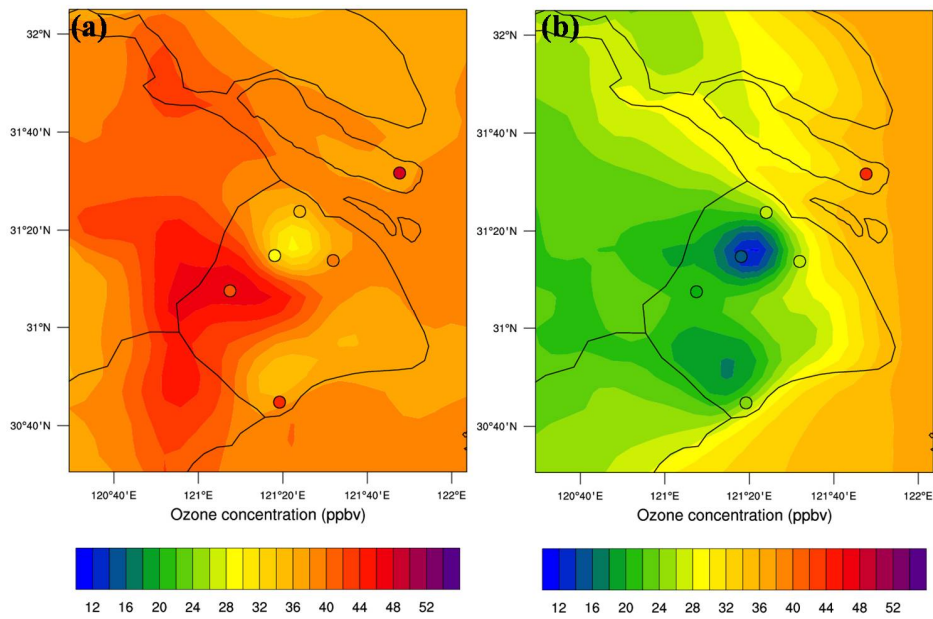
39

40 **(3) Please also add spatial distributions of daytime O<sub>3</sub> and nighttime O<sub>3</sub>**  
41 **in Fig. 8, in addition to mean. Actually mean O<sub>3</sub> can be removed from**  
42 **Fig. 8**

43 Thanks for the suggestion. We calculated the daytime and nighttime O<sub>3</sub>  
44 distribution in September 2009 respectively and compared with  
45 measurements in Fig. 8. The mean daytime and nighttime O<sub>3</sub>

---

46 concentrations in September 2009 are calculated by WRF-Chem and  
47 compared with measurements over 6 sites in Shanghai presented in Fig.  
48 8a and b respectively. Both modeled and measured O<sub>3</sub> concentrations in  
49 daytime are higher than that in nighttime. The calculated daytime O<sub>3</sub>  
50 concentration is about 10-18 ppbv higher than that in nighttime in urban  
51 region (XJH and PD), which is consistent with the measured difference of  
52 12-14 ppbv. In addition, both model simulations and in-situ  
53 measurements in day and nighttime highlight the lower O<sub>3</sub> concentration  
54 in urban zones than that in suburb. The simulated O<sub>3</sub> concentration in  
55 downtown is 28-32 and 12-14 ppbv in daytime and nighttime  
56 respectively, significantly lower than that at sub-urban (36-38 and 26-28  
57 ppbv in daytime and nighttime respectively) and rural (40-42 and 36-38  
58 ppbv in daytime and nighttime respectively), which are well consistent  
59 with the measurements. Above discussion has been included in the  
60 revised version.



61

62 **Figure 8.** The calculated distribution of (a) daytime and (b) nighttime  $O_3$   
 63 concentration by WRF-Chem (shade) in September of 2009 compared  
 64 with measurements (circles) of 6 sites over Shanghai. The minimum  $O_3$   
 65 concentrations in daytime and nighttime both occur in the urban center.  
 66

---

67 **Measurement and model analyses of the ozone variation during 2006 to 2015 and its response**  
68 **to emission change in megacity Shanghai, China**

69  
70 Jianming Xu<sup>1,2</sup>, Xuexi Tie<sup>3,4</sup>, Wei Gao<sup>1,2</sup>, Yanfen Lin<sup>5</sup>, and Qingyan Fu<sup>5</sup>

71  
72 <sup>1</sup> Yangtze River Delta Center for Environmental Meteorology Prediction and Warning, Shanghai  
73 Meteorological Service, Shanghai, 200135, China

74 <sup>2</sup> Shanghai Key Laboratory of Health and Meteorology, Shanghai Meteorological Service, Shanghai,  
75 200135, China

76 <sup>3</sup> Key Laboratory of Aerosol Chemistry & Physics, SKLLQG, Institute of Earth Environment, Chinese  
77 Academy of Science, Xi'an, 710061, China

78 <sup>4</sup> Center for Excellence in Urban Atmospheric Environment, Institute of Urban Environment,  
79 Chinese Academy of Science, Xiamen, 361021, China

80 <sup>5</sup> Shanghai Environmental Monitoring Center, Shanghai, 200135, China

81

82

83

84

85 Correspondence: Xuexi Tie (tiexx@ieecas.cn)

86

---

87        **Abstract.** The fine particles (PM<sub>2.5</sub>) in China decrease significantly in recent years as a result  
88 of the implement of Chinese Clean Air Action Plan since 2013, while the O<sub>3</sub> pollution is getting  
89 worse, especially in megacities such as Beijing and Shanghai. Better understanding the elevated  
90 O<sub>3</sub> pollution in Chinese megacities and its response to emission change is important for  
91 developing an effective emission control strategy in future. In this study, we analyze the  
92 significant increasing trend of daily maximum O<sub>3</sub> concentration from 2006 to 2015 in the  
93 megacity Shanghai with the variability of 0.8-1.3 ppbv yr<sup>-1</sup>. It is likely attributed to the notable  
94 reduction of NO<sub>x</sub> concentration with the decreasing rate of 1.86-2.15 ppbv yr<sup>-1</sup> accompanied with  
95 the little change of VOCs during the same period by excluding the weak trends of meteorological  
96 impacts on local dispersion (wind speed), regional transport (wind direction) and O<sub>3</sub> photolysis  
97 (solar radiation). It is further illustrated by using a state of the art regional chemical/dynamical  
98 model (WRF-Chem) to explore the O<sub>3</sub> variation response to the reduction of NO<sub>x</sub> emission in  
99 Shanghai. The control experiment conducted for September of 2009 shows very excellent  
100 performance for O<sub>3</sub> and NO<sub>x</sub> simulations including both the spatial distribution pattern, and the  
101 day by day variation through comparing with 6 in-situ measurements from MIRAGE-shanghai  
102 field campaign. Sensitive experiments with 30% reduction of NO<sub>x</sub> emission from 2009 to 2015 in  
103 Shanghai estimated by Shanghai Environmental Monitoring Center shows that the calculated O<sub>3</sub>  
104 concentrations exhibit obvious enhancement by 4-7 ppbv in urban zones with the increasing  
105 variability of 0.96-1.06 ppbv yr<sup>-1</sup>, which is well consistent with the observed O<sub>3</sub> trend as a result  
106 of the strong VOC-limited condition for O<sub>3</sub> production. The large reduction of NO<sub>x</sub> combined with  
107 less change of VOCs during the past ten years promotes the O<sub>3</sub> production in Shanghai to move  
108 towards NO<sub>x</sub>-limited regime. Further analysis of WRF-Chem experiments and O<sub>3</sub> isopleths  
109 diagram suggests that the O<sub>3</sub> production in downtown is still under VOC-limited regime after  
110 2015 despite of the remarkable NO<sub>x</sub> reduction, while moves to the transition regime between  
111 NO<sub>x</sub>-limited and VOC-limited in sub-urban zones. Supposing the insignificant VOCs variation  
112 persists, the O<sub>3</sub> concentration in downtown would keep increasing till 2020 with the further 20%  
113 reduction of NO<sub>x</sub> emission after 2015 estimated by Shanghai Clean Air Action Plan. The O<sub>3</sub>  
114 production in Shanghai will switch from VOC-limited to NO<sub>x</sub>-limited regime after 2020 except  
115 downtown area which is likely close to the transition regime. As a result the O<sub>3</sub> concentration will  
116 decrease by 2-3 ppbv in sub-urban zones, and more than 4 ppbv in suburb response to 20%  
117 reduction of NO<sub>x</sub> emission after 2020, whereas is not sensitive to both NO<sub>x</sub> and VOCs changes in  
118 downtown. This result reveals that the control strategy of O<sub>3</sub> pollution is a very complex process,  
119 and needs to be carefully studied.

120  
121        **Key Words:** O<sub>3</sub> pollution in Shanghai, Long-term O<sub>3</sub> trend, WRF-Chem

122

---

123 **1 Introduction**

124 Ozone (O<sub>3</sub>) in the troposphere plays the important role in the oxidation of chemically and  
125 climatically relevant trace gases, hence regulating their lifetime in the atmosphere (Monks et al.,  
126 2015). In the lower troposphere, O<sub>3</sub> is produced from photochemical reactions involving volatile  
127 organic compounds (VOCs, broadly including CO) and nitrogen oxides (NO<sub>x</sub> = NO + NO<sub>2</sub>) in the  
128 presence of sunlight (Brasseur et al., 1999). As a strong oxidant, O<sub>3</sub> at ground level is detrimental  
129 to human health and vegetation (Tai et al., 2014), and has been received continuous attention  
130 from both the scientific and regulatory communities in the past three decades.

131 Shanghai has emerged as one of the largest megacities in the world over the last two  
132 decades. The city has a fleet of over 3.6 million vehicles and the population of over 2400 million  
133 permanent residents, which results in high emissions of NO<sub>x</sub>, VOCs, and primary particulate  
134 matter (PM) to the atmosphere from industrial and commercial activities, leading to the  
135 photochemical smog formation. Persistent high level of surface O<sub>3</sub> and PM were observed in  
136 Shanghai during the past ten years (Geng et al., 2007; Ran et al., 2009; Tie et al., 2009a; Xu et al.,  
137 2015). In order to mitigate the adverse impacts from severe air pollution, the Clean Air Action  
138 Plan was issued in the end of 2013 to implement the emission reduction program in Shanghai  
139 and its neighboring area. As a result, the annual mean PM<sub>2.5</sub> (particles with diameter  $\leq$  2.5  $\mu$ m)  
140 mass concentration has decreased from 50  $\mu$ g m<sup>-3</sup> in 2013 to 39  $\mu$ g m<sup>-3</sup> in 2017. However O<sub>3</sub>  
141 pollution has been continuously worsen, with the non-attainment days (daily maximum O<sub>3</sub>  
142 concentration exceeding 200  $\mu$ g m<sup>-3</sup>, or daily maximum 8h-O<sub>3</sub> concentration exceeding 100  $\mu$ g m<sup>-3</sup>)  
143 increased from 99 d in 2014 to 129 d in 2016. As a result, O<sub>3</sub> becomes the primary air pollutant  
144 affecting the ambient air quality instead of PM<sub>2.5</sub> in Shanghai. Similar issue has also been  
145 occurred in other cities in the eastern China (Lu et al., 2018). For example, the mean PM<sub>2.5</sub> mass  
146 concentration over the 74 major cities decreased by 40% from 2013 to 2017, whereas the  
147 maximum daily 8-h average O<sub>3</sub> concentration in summer exceeds the Chinese National Ambient  
148 Air Quality Standard (GB3095-2012) over most of eastern China (Li et al., 2019). Thus better  
149 understanding the causes of elevated O<sub>3</sub> in China is important for developing effective O<sub>3</sub> control  
150 strategies, especially in megacities such as Shanghai.

151 A prerequisite to an effective emission-based O<sub>3</sub> control strategy is to understand the  
152 temporal and spatial relationship between O<sub>3</sub> and its precursors, and the response of O<sub>3</sub>  
153 concentrations to the changes in emissions of O<sub>3</sub>-precursors (such as NO<sub>x</sub> and VOCs, Lin et al.,  
154 1988). The relationship of O<sub>3</sub> and O<sub>3</sub>-precursors can be clarified as NO<sub>x</sub>-limited or VOC-limited  
155 chemistry of O<sub>3</sub> formation, which is usually defined based on the relative impact of a given  
156 percent reduction in NO<sub>x</sub> relative to VOCs in the context of urban chemistry (Sillman, 1999).

157 Some observational and modeling works on O<sub>3</sub> chemical formation and transformation have  
158 been carried out in Shanghai since 2007. The O<sub>3</sub> production in Shanghai city is clearly under  
159 VOC-limited regime (Geng et al., 2007), in which the aromatics and alkenes play the dominant  
160 roles (Geng et al., 2008a). The aircraft measurements in Yangtze River Delta (YRD) region show  
161 the strong anti-correlation between NO<sub>x</sub> and O<sub>3</sub> during noontime, indicating the similar  
162 VOC-limited regime for O<sub>3</sub> production in the area neighboring Shanghai (Geng et al., 2008b). Thus  
163 either NO<sub>x</sub> reduction or VOCs growth is favorable for O<sub>3</sub> enhancement in Shanghai. Gao et al.  
164 (2017) reported that O<sub>3</sub> concentration in Shanghai downtown increased 67% from 2006 to 2015,  
165 whereas NO<sub>x</sub> concentration decreased about 38%. This is also consistent with the results of Lin et  
166 al. (2017) that, the median of the maximum daily 8-h average O<sub>3</sub> concentration in Shanghai



---

167 increased notably from 2006 to 2016, with the rate of  $1.4 \text{ ppbv yr}^{-1}$ , while the  $\text{NO}_2$  decreased  
168 from  $66.7$  to  $42.1 \text{ }\mu\text{g m}^{-3}$  with about 20% reduction. These previous studies provide the useful  
169 information regarding the  $\text{O}_3$  chemical formation and transformation in Shanghai. However, such  
170  $\text{O}_3$  variation responding to emission change has not been clearly investigated. Considering that  $\text{O}_3$   
171 formation is a complicated process including chemistry, transport, emission, deposition and their  
172 interactions, the chemical transport model is the powerful tool to gain an understanding of these  
173 interacting processes. For example, Lei et al. (2007), Ying et al. (2009) and Song et al. (2010)  
174 investigated the  $\text{O}_3$  production rate and its sensitivity to emission changes of  $\text{O}_3$  precursors by  
175 CAMx model in Mexico City Metropolitan Area (MCMA). Tie et al. (2013) analyzed the  
176 comprehensive data of the MIRAGE-Shanghai field campaign by WRF-Chem model, and  
177 quantified the threshold value by the emission ratio of  $\text{NO}_x/\text{VOCs}$  for switching from VOC-limited  
178 to  $\text{NO}_x$ -limited in Shanghai. Recently Li et al. (2019) suggested an important cause of the  
179 increasing  $\text{O}_3$  in North China Plain (NCP) during 2013 to 2017 as the significant decrease in  $\text{PM}_{2.5}$   
180 slowing down the sink of hydroperoxy radicals and thus speeding up the  $\text{O}_3$  production by  
181 GOES-CHEM model. However such implication for  $\text{O}_3$  trend is not pervasive in YRD and other  
182 regions. Moreover, the 5-year  $\text{O}_3$  records seem rather short to examine the inter-annual  
183 variability of  $\text{O}_3$  concentration. The GOES-CHEM experiment with 50 km resolution maybe is  
184 suitable for the  $\text{O}_3$  simulation at regional scale but is too coarse to resolve the local  $\text{O}_3$  budget at  
185 urban scale, such as Beijing or Shanghai. To our knowledge, there are no peer-reviewed modeling  
186 studies focus on the past long term  $\text{O}_3$  variations response to emission changes conducted in  
187 Shanghai. Thus this paper extends the study of Tie et al. (2013) and Gao et al. (2017) to not only  
188 further examine the inter-annual  $\text{O}_3$  variations from a larger scale with more comprehensive  
189 measurements, but also explore the  $\text{O}_3$  enhancement response to  $\text{NO}_x$  reduction in Shanghai and  
190 predict the future  $\text{O}_3$  variations by models. The effects of emission changes on long term  $\text{O}_3$   
191 variability are evaluated by WRF-Chem model with high resolution and compared with  
192 measurements. The shift of  $\text{O}_3$  photochemical regime relative to the variations of  $\text{NO}_x$  and VOCs  
193 concentrations in the past ten years is discussed by  $\text{O}_3$  isopleths diagram combined with  
194 WRF-Chem model to provide more insights into the  $\text{O}_3$  control strategy. Moreover, the future  $\text{O}_3$   
195 levels and its possible chemical regime in Shanghai are also discussed according to the Shanghai  
196 Clean Air Action Plan.

197 The paper is constructed as follows. The measurements and models used for this study are  
198 described in Sect. 2. The analysis on the long-term in-situ measurements of  $\text{O}_3$  and its precursors,  
199 as well as the model sensitive experiments are presented and discussed in Sect. 3-6. The  
200 conclusion is summarized in Sect. 7.

201

## 202 **2 Measurements and models**

### 203 **2.1 Measurements**

204 The measurements of  $\text{O}_3$  and  $\text{NO}_x$  are collected from 6 sites (XJH, PD, JS, BS, SS, DT) over  
205 Shanghai (Fig. 1 a) under different influence of air pollutant emissions. The XJH site is located at  
206 the downtown of Shanghai, which is strongly influenced by emission of transportation. The PD  
207 site is located at the sub-urban area near a big park, which is influenced by the mixed emissions  
208 of transportation and residential. The JS site is located in the south of Shanghai with several large  
209 chemical industries. The BS site is located in the north of Shanghai with some big steel and power

---

210 plants. The SS site is located at the top of the sole hill (100 m a.g.l) in Shanghai, which has minor  
211 effect from local emissions, and is influenced by regional transport. The DT site is located at a  
212 remote island without anthropogenic activities. These O<sub>3</sub> and NO<sub>x</sub> measurements are used for  
213 the evaluation on WRF-Chem performance. In addition, the VOCs are sampled at the downtown  
214 site XJH and the sub-urban site PD, and are analyzed at a chemistry laboratory. The study on the  
215 O<sub>3</sub> chemical production in this paper is limited at XJH and PD by the intensive measurements of  
216 O<sub>3</sub> and its precursors (VOCs and NO<sub>x</sub>) from 2006 to 2015. The meteorological measurements  
217 including wind speed and direction, solar radiation and temperature are collected at BS site,  
218 which is the only climatology observatory in Shanghai. The meteorological measurements in BS  
219 are used for international exchange of meteorological data representing Shanghai, sponsored by  
220 the World Meteorological Organization (WMO).

## 221 **2.2 Instruments**

222 O<sub>3</sub> is measured using an EC 9810 Ozone Analyzer, together with a UV photometer, which  
223 accurately and reliably measures O<sub>3</sub> concentration in ambient air. The oxides of nitrogen analyzer  
224 (EC9841B/ECOTECH) have a heated molybdenum NO<sub>2</sub> to NO converter. The resulting NO  
225 concentration is quantified using the chemiluminescence technique. This instrument has  
226 automated to set to be zero, and include an optional external valve manifold and external  
227 calibration sources. Quality control checks are performed every 3 days, including inspection of  
228 the shelter and instruments as well as zero, precision and span checks. Filter is replaced once  
229 every two weeks and calibration is made every month. The O<sub>3</sub> concentrations are recorded every  
230 1 min.

231 VOCs concentrations are sampled for 24 h every day with a 6 L silonite canister with a  
232 silonite coated valve (model 29-10622). The internal silonite coating improves long-term VOC  
233 storage. The instrument has a large volume to detect volatile chemicals down to low pptv range.  
234 Absorption is eliminated by using nupropackless valves and by eliminating teflon tape in the valve  
235 stem. These canisters are recognized to meet or exceed the technical specifications required for  
236 EP methods TO14-A and TO15. Gases samples are pre-processed using Model 7100 VOC  
237 preconcentrator. Samples are analyzed for VOCs using a gas chromatography system (Agilent  
238 GC6890) coupled with mass-selective detection (Agilent MSD5975 N) with length of 60 m,  
239 diameter of 0.32 mm, and film thickness of 1.0 μm. This measurement system can detect VOCs  
240 concentrations down to low pptv range.

241 These instruments to measure O<sub>3</sub>, NO<sub>x</sub> and VOCs concentrations are calibrated carefully.  
242 Detail information for the instruments and the procedures to perform data quality control are  
243 described by Geng et al. (2007), Ran et al. (2009), Tie et al. (2013) and Gao et al. (2017). These  
244 data have been widely used to investigate the diurnal, seasonal and inter-annual variations of O<sub>3</sub>  
245 in Shanghai (Geng et al., 2007; 2015; Tang et al., 2008; Ran et al., 2009; Gao et al., 2017) and its  
246 chemical mechanism (Geng et al., 2008a; 2008b; Tie et al., 2009a; 2013).

## 247 **2.3 WRF-Chem model**

248 The regional chemical/transport model (Weather Research and Forecasting Chemical model-  
249 WRF-Chem) (Grell et al., 2005) is used to investigate the O<sub>3</sub> variations response to emission  
250 changes in Shanghai. The version of the model is improved mainly by Tie et al. (2007) and Li et al.  
251 (2010; 2011). The chemical mechanism chosen in WRF-Chem is the RADM2 (Regional Acid

---

252 Deposition Model, version 2) gas-phase chemical mechanism (Stockwell et al., 1990), which  
253 includes 158 reactions among 36 species. The fast radiation transfer module (FTUV) is developed  
254 and used to calculate photolysis rates (Tie et al., 2003), considering the impacts of aerosols and  
255 clouds on the photochemistry (Li et al., 2011). The aerosol modules are developed by EPA CMAQ  
256 (version 4.6) (Binkowski and Roselle, 2003). The wet deposition of chemical species is calculated  
257 using the method in the CMAQ module and the dry deposition parameterization follows Wesely  
258 et al. (1989). The ISORROPIA version 1.7 is used to calculate the inorganic aerosols (Nenes et al.,  
259 1998). The secondary organic aerosol (SOA) is predicted using a non-traditional SOA module,  
260 including the volatility basis set (VBS) modeling approach in which primary organic components  
261 are assumed to be semi-volatile and photochemically reactive and are distributed in  
262 logarithmically spaced volatility bins. The partitioning of semi-volatile organic species is  
263 calculated supposing the bulk gas and particle phases are in equilibrium and all condensable  
264 organics form a pseudoideal solution. Nine surrogate species with saturation concentrations from  
265  $10^{-2}$  to  $10^6 \mu\text{g m}^{-3}$  at room temperature are used for the primary organic aerosol (POA)  
266 components. The SOA contributions from glyoxal and methylglyoxal is also included. The major  
267 physical processes employed in WRF are summarized as the Lin microphysics scheme (Lin et al.,  
268 1983), the Yonsei University (YSU) PBL scheme (Hong et al., 2006), the Noah Land surface model  
269 (Chen and Dudhia, 2001), and the long wave radiation parameterization (Dudhia, 1989).

270 The domain is set up to cover a region (centered at  $32.5^\circ\text{N}$ ,  $118^\circ\text{E}$ ) of  $356 \times 345$  grids with  
271 a horizontal resolution of 6 km (Zhou et al., 2017). The initial and lateral boundary conditions of  
272 the meteorology are extracted from the NCEP FNL reanalysis data. The lateral meteorological  
273 boundary is updated every 6 h. The chemical lateral boundary conditions are constrained by the  
274 global chemical transport model (MOART–Model for Ozone and Related chemical Tracers) with  
275 aerosol formation modules (Tie et al., 2001; Emmons et al., 2010). Both the chemical and  
276 dynamical integration step is set as 60 s. The Multi-resolution Emission Inventory for China (MEIC)  
277 developed by Zhang et al. (2009) is used in WRF-Chem for the domain except Shanghai with  $0.25^\circ$   
278 resolution. The anthropogenic emissions (including  $\text{CO}$ ,  $\text{NO}_x$ ,  $\text{SO}_2$  and VOCs) for Shanghai are  
279 developed by Tie et al. (2013) with  $0.16^\circ$  resolution based on the MIRAGE-shanghai field  
280 campaign.  $\text{NO}_x$  and  $\text{SO}_2$  emissions in YRD region are adjusted by Zhou et al. (2017) according to  
281 the performance evaluation of WRF-Chem prediction for about 195 cities during 2014-2015. The  
282 distribution of  $\text{NO}_x$  emission in 2009 in Shanghai is depicted in Fig. 1b. The biogenic emissions are  
283 calculated online using the MEGAN (Model of Emissions of Gases and Aerosol from Nature)  
284 model developed by Guenther et al. (2006).

285

286 **Figure 1.** (a) The distribution of land-use category in Shanghai. The blue dots denote the locations  
287 of 6 sites (XJH, BS, PD, SS, JS, DT). (b) The  $\text{NO}_x$  emission of 2009 scenario in Shanghai.

#### 288 **2.4 OZIPR model**

289 The ozone isopleths diagram for Shanghai is plotted by OZIPR (Ozone Isopleths Plotting Package  
290 Research) model (Gery and Crouse, 2002). The OZIPR model employs a trajectory-based air  
291 quality simulation model in conjunction with the Empirical Kinetics Modeling Approach (EKMA)  
292 to relate  $\text{O}_3$  concentrations levels of organic and nitrogen oxide emissions. OZIPR simulates  
293 complex chemical and physical processes of the lower atmosphere through a trajectory model.  
294 The physical representation is a well-mixed column of air extending from the ground to the top of

---

295 the mixed layer. Emissions from the surface are included as the air column passes over different  
296 emission sources, and air from above the column is mixed in as the inversion rises during the day.  
297 O<sub>3</sub> precursor concentrations and ambient information such as temperature, relative humidity and  
298 boundary layer height from measurements in Shanghai were specified for each single run.  
299 Therefore a series of simulations were performed to calculate peak O<sub>3</sub> concentration as a  
300 function of initial precursor concentrations (Tang et al., 2008; Geng et al., 2008b).

301

### 302 **3 Variability of O<sub>3</sub> and its precursors measured in Shanghai**

#### 303 **3.1 Variation of O<sub>3</sub> concentration**

304 Fig. 2a and b show the annual variation of daily maximum O<sub>3</sub> concentration at downtown site XJH  
305 and sub-urban site PD respectively from 2006 to 2015. The daily maximum O<sub>3</sub> concentrations  
306 increase notably during the past ten years with the increasing rate of 0.808 ppbv yr<sup>-1</sup> at XJH and  
307 1.374 ppbv yr<sup>-1</sup> at PD respectively. In similar the daily maximum 8h-O<sub>3</sub> concentration also  
308 increased at the rate of 1.06 and 1.4 ppbv yr<sup>-1</sup> respectively. It is consistent with the reported O<sub>3</sub>  
309 increasing trend ranging from 1-2 ppbv yr<sup>-1</sup> at background and urban sites in eastern China during  
310 2001 to 2015 (Tang et al., 2009; Ma et al., 2016; Sun et al., 2016). In 2006, the mean daily  
311 maximum O<sub>3</sub> concentrations at XJH and PD are 25.2 ppbv and 32.7 ppbv respectively. While in  
312 2017, the mean daily maximum O<sub>3</sub> concentrations at the two sites increase to 41.3 ppbv and 51.8  
313 ppbv respectively, with 64% and 58% enhancement compared with that in 2006. The mean daily  
314 maximum O<sub>3</sub> concentration at downtown site XJH during 2006 to 2015 is 39.2 ppbv, which is  
315 significantly lower than that at sub-urban site PD of 50.7 ppbv, suggesting the O<sub>3</sub> is depressed in  
316 downtown area. Geng et al. (2007) suggested that the O<sub>3</sub> production in the city of Shanghai was  
317 under VOC-limited regime, thus higher NO<sub>x</sub> in downtown resulted in lower O<sub>3</sub> concentration.  
318 Considering the inhomogeneous spatial distribution of the precursors of O<sub>3</sub> in Shanghai (Geng et  
319 al. 2008a), we extend the analysis on O<sub>3</sub> variations to a broader scope by using the O<sub>3</sub>  
320 measurements from 31 sites provided by Shanghai Environmental Monitoring Center, covering  
321 the entire Shanghai area. It is shown in Fig. 2c that the median of the O<sub>3</sub>-8h concentration also  
322 increases significantly from 2006 to 2015, with the increasing rate of 1.571 ppbv yr<sup>-1</sup>, indicating  
323 that the significant increasing trend of O<sub>3</sub> concentration not only occurs in the city of Shanghai,  
324 but also expanded to a larger area nearby Shanghai. Li et al. (2019) also reported a regional O<sub>3</sub>  
325 increasing phenomena in summer during 2013 to 2017 from Shanghai to Beijing in eastern China.

326 In order to analyze the individual contribution to the long-term O<sub>3</sub> trend, the variations of O<sub>3</sub>  
327 precursors, and meteorological parameters are measured and showed in the following sections.

328

329 **Figure 2.** The annual variation of daily maximum O<sub>3</sub> concentration (ppbv) from 2006 to 2015 at (a)  
330 downtown site XJH and (b) sub-urban site PD, both presenting the significant increasing trends  
331 with 0.808 ppbv yr<sup>-1</sup> at XJH and 1.374 ppbv yr<sup>-1</sup> at PD. The variation of the median 8-h O<sub>3</sub>  
332 concentration (ppbv) from 2006 to 2015 averaged for 31 sites over Shanghai (c), also shows the  
333 increasing variability of 1.571 ppbv yr<sup>-1</sup>.

#### 334 **3.2 Variations of the precursors (NO<sub>x</sub> and VOCs)**

335 It is well known that the tropospheric O<sub>3</sub> formation is throughout a complicated photochemical  
336 process, and is strongly related to the precursors of O<sub>3</sub> (VOCs and NO<sub>x</sub>). According to the previous

---

337 studies (Geng et al., 2007; Ran et al., 2009), the chemical formation of O<sub>3</sub> in Shanghai is revealed  
338 to be under VOC-limited. Thus either enhancement of VOCs or reduction in NO<sub>x</sub> would both  
339 result in the growth of O<sub>3</sub> concentration. In order to better understanding the factors possibly  
340 driving the O<sub>3</sub> increasing trend depicted in Fig. 2, the variations of NO<sub>x</sub> and VOCs concentrations  
341 at XJH and PD in the same period are presented in Fig. 3. The NO<sub>x</sub> concentrations present  
342 significant decreasing trend from 2006 to 2015 at both XJH and PD sites, which is opposite to the  
343 increasing trend of O<sub>3</sub> variations in Fig. 2. At XJH, the decreasing rate of NO<sub>x</sub> is 2.15 ppbv yr<sup>-1</sup>,  
344 which is more remarkable than that at PD site of 1.86 ppbv yr<sup>-1</sup>. According to the studies by Lin et  
345 al (2017), the reduction of NO<sub>x</sub> concentration in Shanghai was likely attributed to the  
346 implementation of stringent emission control strategy for transportation, including improvement  
347 of gas quality, popular usage of electricity cars, and limitation of heavy cars into the urban zones.  
348 These regulations significantly decrease the emissions of NO<sub>x</sub> into the atmosphere, resulting in  
349 lower NO<sub>x</sub> concentrations. Zheng et al. (2018) also reported the 30% reduction of NO<sub>x</sub> emission in  
350 the past 5 years in YRD region. In comparison, the VOCs concentrations at XJH and PD decrease  
351 very slightly during 2006 to 2015. At XJH, the mean VOCs concentration during 2013 to 2015 is  
352 about 20 ppbv, which is some lower than that during 2009 to 2012 of 23 ppbv. At PD, the VOCs  
353 concentration shows strong inter-annual variations, ranging from 16 to 22 ppbv. Generally the  
354 VOCs concentration at the downtown site XJH is higher than that at the sub-urban site PD by 14%.  
355 It is consistent with the studies of Cai et al. (2010), suggesting that about 25% of VOCs is  
356 attributed to the vehicles in shanghai urban zones.

357

358 **Figure 3.** The mean annual concentrations (ppbv) of NO<sub>x</sub> (dots) and VOCs (bars) from 2006 to  
359 2015 at (a) downtown site XJH and (b) sub-urban site PD respectively. The NO<sub>x</sub> concentrations at  
360 XJH and PD both present obvious decreasing trends with -2.1 ppbv yr<sup>-1</sup> and -1.87 ppbv yr<sup>-1</sup>. While  
361 the VOCs concentrations at both sites present no clear inter-annual trends.

362

### 363 3.3 Meteorological impacts on O<sub>3</sub> photolysis, dispersion and transport

364 In addition to the precursors, meteorology such as solar radiation and wind speed and directions  
365 also plays the important roles in O<sub>3</sub> concentration through the photochemical and physical  
366 processes. Fig. 4 shows the annual variation of wind speed and total solar radiation from 2006 to  
367 2015. The solar radiation presents weak annual variations ranging from 140 to 150 Wm<sup>-2</sup>,  
368 exhibiting a large variability but without a significant trend. As a result, the variation of solar  
369 radiation cannot explain the significant change of O<sub>3</sub> concentration on the view of photolysis. The  
370 wind speed is usually regarded as the indicator for the dispersion capacity for air pollutants.  
371 Several studies reported that the wind speed in winter in eastern China presented decreasing  
372 variability during the past 40 years due to the decadal variation of winter monsoon affecting the  
373 haze occurrence (Wang et al., 2016; Zhao et al., 2016; Xu et al., 2017). While high O<sub>3</sub> events  
374 usually occur in summer season for middle-latitude cities such as Shanghai (Wang et al., 2017).  
375 The mean summer wind speed in Fig. 4a fluctuates between 3.3 ms<sup>-1</sup> to 3.9 ms<sup>-1</sup> during 2006 to  
376 2015 except the minimum value in 2014 (2.9 ms<sup>-1</sup>) due to fewer typhoon in the period. Without  
377 2014, the variability of summer wind speed is insignificant, with a trend of -0.02 m s<sup>-1</sup> yr<sup>-1</sup>, which  
378 could not be regarded as the dominant factor to interpret the increasing O<sub>3</sub> trend. Local O<sub>3</sub>  
379 concentration would be affected by transport of upstream plumes usually determined by wind

380 direction. Geng et al. (2011) suggested that O<sub>3</sub> concentration was higher in west wind compared  
381 with other wind sectors in Shanghai indicating the possible O<sub>3</sub> transport from western area out of  
382 Shanghai. Fig. 5 presents the annual wind rose at Baoshan site from 2006 to 2015, presenting the  
383 very similar pattern of wind direction in each year. The mean wind direction concentrates in the  
384 sector between 60-80 degree, suggesting the dominant wind in Shanghai is easterly accounting  
385 for 50%. The east wind in Shanghai usually carries with the clean air mass from the sea to  
386 improve the local air quality (Xu et al., 2015). The frequency of west wind changes little during  
387 2006 and 2015 ranging from 10-15%, suggesting that the regional transport is not a major factor  
388 driving the O<sub>3</sub> increasing. Based on the above analysis, it is speculated that the rapid O<sub>3</sub>  
389 increasing during 2006–2015 in shanghai is likely attributed to the reduction of NO<sub>x</sub>  
390 concentration as a result of the VOC-limited condition for O<sub>3</sub> production.

391 **Figure 4.** The annual variation of (a) summer wind speed (m s<sup>-1</sup>) and (b) total solar radiation (W  
392 m<sup>-2</sup>) from 2006 to 2015 in Shanghai. Both wind speed and the solar radiation present weak  
393 inter-annual variations but without significant trends.  
394

395 **Figure 5.** The wind rose in each year from 2006 to 2015 in Shanghai. The red line means the  
396 resultant vector suggesting the dominant wind direction.  
397  
398

### 399 3.4 Different O<sub>3</sub> variability in nighttime and daytime

400 The mean diurnal variations of O<sub>3</sub> concentrations in 2006 and 2015 are compared in Fig. 6a at XJH  
401 and PD sites respectively. The maximum and minimum O<sub>3</sub> concentrations occur in the afternoon  
402 (14-15 pm) and in the early morning (6-7 am) respectively at both sites. In addition, the diurnal  
403 O<sub>3</sub> concentrations at XJH and PD all increase significantly from 2006 to 2015. For example, the  
404 peak O<sub>3</sub> concentration at XJH increases from 21 ppbv to 37 ppbv, meanwhile the minimum O<sub>3</sub>  
405 concentration rises from 5 ppbv to 14 ppbv exhibiting higher increasing rate. Similar diurnal O<sub>3</sub>  
406 enhancement is also observed at PD site during the same period. The O<sub>3</sub> chemical mechanism in  
407 daytime includes both production and loss processes. In contrast, in nighttime, the  
408 photochemical production ceases, and there mainly exists loss process for O<sub>3</sub>. In addition both  
409 dry deposition and nighttime turbulence also have the influence in the nighttime O<sub>3</sub>  
410 concentration according to the work by Hu et al. (2013). Fig. 6b shows the trends of hourly annual  
411 O<sub>3</sub> variability change rate of the diurnal O<sub>3</sub> concentration from 2006 to 2015 at XJH and PD sites  
412 respectively. The O<sub>3</sub> concentrations present increasing trends both in daytime (8:00-18:00, LST)  
413 and nighttime (19:00-07:00, LST) at XJH and PD sites, which is consistent with the results in Fig. 2.  
414 The nighttime O<sub>3</sub> concentrations increase more significantly than daytime O<sub>3</sub> at XJH, with the  
415 increasing rate of 1.239 and 0.956 ppbv yr<sup>-1</sup> respectively. While at PD site the O<sub>3</sub> concentrations  
416 increase by 1.338 ppbv yr<sup>-1</sup> in daytime which is higher than that in nighttime by 1.028 ppbv yr<sup>-1</sup>.  
417 In comparison, the nighttime O<sub>3</sub> concentrations exhibit higher increasing rate at downtown site  
418 XJH than that at sub-urban site PD due to more NO emissions or more intensified urbanization  
419 (Hu et al., 2013) at urban center. These results suggest that the reduction of NO<sub>x</sub> concentration  
420 from 2006 to 2015 has different effects on daytime and nighttime O<sub>3</sub> variations. The O<sub>3</sub>  
421 concentration in nighttime is more sensitive to NO<sub>x</sub> reduction at downtown site, resulting in less  
422 O<sub>3</sub> lost compared with that in daytime. The results in Fig. 6b also show that the increasing rate of

带格式的：下标

带格式的：下标

带格式的：下标

带格式的：下标

带格式的：下标

带格式的：下标

带格式的：下标

423 nighttime O<sub>3</sub> in downtown site XJH is higher than that at sub-urban site PD due to the more  
424 reduction of NO<sub>x</sub> concentration in downtown area. Furthermore, the seasonal variability of  
425 daytime and nighttime O<sub>3</sub> concentrations at XJH site are illustrated in Fig. 7. Both daytime and  
426 night O<sub>3</sub> concentrations present increasing trends in all seasons. In comparison, the larger  
427 increasing rates of nighttime O<sub>3</sub> concentration are observed in spring, summer and autumn than  
428 that in daytime. For example, the nighttime O<sub>3</sub> concentrations increase at 1.341, 1.159 and 1.525  
429 ppbv yr<sup>-1</sup> in spring, summer and autumn respectively, which are more significant than that of  
430 1.008, 0.378 and 1.370 ppbv yr<sup>-1</sup> in daytime. The variability of winter O<sub>3</sub> concentrations in  
431 daytime and nighttime are generally close perhaps due to the lower O<sub>3</sub> photochemical  
432 productions. –Hu et al. (2016) suggested that the nighttime boundary layer tended to be less  
433 stable resulted from the enhanced sensible heat flux in urban area, thus leading to more active  
434 nighttime turbulence. The sounding measurements at 20:00 (LST) in Shanghai are used to  
435 calculate the vertical temperature gradient between 1000 hPa and 925 hPa to indicate the  
436 intensity of nighttime turbulence, while presenting no significant trend from 2010 to 2015.  
437 Furthermore the PBL height retrieved from Lidar measurements at 20:00 (LST) presents the  
438 similar results as soundings. Based on the above measurements, the variation of turbulence at  
439 night may have only minor contribution to the nighttime O<sub>3</sub> increasing in Shanghai. However the  
440 effect of dry deposition could not be excluded by lacking of measurements, which need further  
441 investigation.

442

443 Figure 6. (a) The mean diurnal variation of O<sub>3</sub> concentration (ppbv) compared between 2006 and  
444 2015 in XJH (red dots) and PD (blue dots). (b) The annual change rate of diurnal O<sub>3</sub> concentration  
445 (ppbv.yr<sup>-1</sup>) from 2006 to 2015 at downtown site XJH (red bars) and sub-urban site PD (blue  
446 bars). Figure 6. The variability of hourly O<sub>3</sub> concentration from 2006 to 2015 at downtown site XJH  
447 (red bars) and sub-urban site PD (blue bars).

448

449 **Figure 7.** The daytime (8:00-18:00, LST) and nighttime (19:00-07:00, LST) O<sub>3</sub> variability from 2006  
450 to 2015 at downtown site XJH in (a) spring, (b) summer, (c) autumn and (d) winter.

451

#### 452 **4 WRF-Chem study on the O<sub>3</sub> variation response to emission change**

##### 453 **4.1 Design of the model experiments scheme**

454 To better understand the role of NO<sub>x</sub> emission reduction in O<sub>3</sub> variation, the WRF-Chem model is  
455 utilized to calculate the changes of O<sub>3</sub> concentrations. Lin et al. (2017) suggested that the NO<sub>x</sub>  
456 emission was reduced in Shanghai in recent years resulted from the implementation of the  
457 Shanghai Clean Air Action Plan. The NO<sub>x</sub> emission in 2015 is estimated at 33.4×10<sup>4</sup> ton in  
458 Shanghai, reduced significantly by 30% compared with that in 2009 of 44.9×10<sup>4</sup> ton. Thus it  
459 provided the good opportunity to examine the O<sub>3</sub> variation response to the reduction of NO<sub>x</sub>  
460 emission in Shanghai. The NO<sub>x</sub> emissions in 2009 and 2015 are put into WRF-Chem model  
461 respectively to calculate the O<sub>3</sub> concentration. The other emissions (including gas and particulate  
462 matter) and meteorology used in WRF-Chem are set to be same. As a result, the difference of O<sub>3</sub>  
463 concentrations calculated by WRF-Chem is solely attributed to the change of NO<sub>x</sub> emission  
464 between 2009 and 2015, which is furthermore compared with the measurements.

465 The MIRAGE-shanghai field campaign was conducted in September of 2009 to explore the

---

466 O<sub>3</sub> chemical formation and transformation in Shanghai (Tie et al., 2013). The mean temperature,  
467 mean wind speed and total precipitation in this month is 25 °C, 2.85 m s<sup>-1</sup> and 89.5 mm  
468 respectively, which is very close to the climatological conditions during the past ten years from  
469 2006 to 2015, with 24.7 °C for mean temperature, 2.81 m s<sup>-1</sup> for mean wind speed, and 126 mm  
470 for total precipitation respectively. In addition, Shanghai is located at the typical sub-tropical area.  
471 The meteorology in September is characterized as the low cloud cover and rain occurrence, the  
472 slight wind speed and humidity, as well as the moderate solar radiation intensity. As suggested by  
473 Tie et al. (2013), the chemical age of O<sub>3</sub> plume in Shanghai urban area in September of 2009 was  
474 very young, indicating that the O<sub>3</sub> production was more dependent on the local emissions under  
475 such kind of meteorology, hence providing more insights into the O<sub>3</sub> chemical mechanism  
476 response to the local emission changes. We chose the meteorology in September of 2009 as the  
477 atmospheric background for all the sensitive experiments by WRF-Chem.

478 Tie et al. (2009a; 2013) highlighted that the WRF-Chem model was capable of studying the  
479 chemical and physical processes of O<sub>3</sub> in September of 2009 during the MIRAGE-Shanghai  
480 campaign. The calculated O<sub>3</sub>, NO<sub>x</sub>, VOCs and aerosols by WRF-Chem in clean and polluted  
481 episodes are fairly in agreement with the measurements except HONO, suggesting that the  
482 emission inventory in 2009 used in the model is reasonable for the Shanghai region. Moreover  
483 the VOCs emission in Shanghai is greatly improved according to the measurements from the  
484 MIRAGE-shanghai field campaign by Tie et al. (2013). Such emission from Tie et al. (2013)  
485 representing 2009 scenario is used in this study to conduct the control experiment (T1) as the  
486 baseline to simulate the O<sub>3</sub> and NO<sub>x</sub> concentrations in September of 2009. The T1 experiment is  
487 composed of 30 model runs for each day in September of 2009. Each model run is initiated at the  
488 20:00 (LST) and performed for 52 h integrations. The first 28 h integration is regarded as model  
489 spin-up periods, the results from the later 24 h integration is captured hourly and averaged for  
490 mean daily concentration of O<sub>3</sub> and NO<sub>x</sub>. The aim of the T1 experiment is to further evaluate the  
491 reliability of the emission inventory in 2009 used in WRF-Chem by fully comparing the calculated  
492 O<sub>3</sub> and NO<sub>x</sub> concentrations with in-situ measurements of 6 sites over Shanghai.

#### 493 **4.2 The NO<sub>x</sub> emission in 2009 used for base experiment**

494 The distribution of NO<sub>x</sub> emission of 2009 scenario (Tie et al., 2013) in Shanghai used in  
495 WRF-Chem model has been showed in Fig. 1b. The NO<sub>x</sub> emission is mostly distributed in the  
496 urban zones, suggesting that transportation is the important source. The NO<sub>x</sub> is largely exported  
497 in downtown and two neighboring sub-urban zones in the east and north respectively. The  
498 maximum NO<sub>x</sub> emission is estimated at 16 kg hr<sup>-1</sup> km<sup>-2</sup> at downtown, compared with 2-6 kg hr<sup>-1</sup>  
499 km<sup>-2</sup> in the sub-urban area. In addition, there is a small town located in the south of Shanghai  
500 with the similar intensity of NO<sub>x</sub> emission as the sub-urban zones. The total NO<sub>x</sub> emission of 2009  
501 scenario in Shanghai (Fig. 1b) is estimated at 41.4 × 10<sup>4</sup> ton in the model, which is close to the  
502 47.8 × 10<sup>4</sup> ton suggested by Lin et al. (2017) according to the Shanghai Environmental Year Book.

#### 503 **4.3 Performance evaluation on the base experiment**

504 The mean ~~monthly daytime and nighttime~~ O<sub>3</sub> concentrations in September 2009 ~~are~~ calculated  
505 by WRF-Chem and compared with measurements over 6 sites in Shanghai presented in Fig. 8a  
506 and b respectively. Both modeled and measured O<sub>3</sub> concentrations in daytime are higher than  
507 that in nighttime. The calculated daytime O<sub>3</sub> concentration is about 10-18 ppbv higher than that



508 | in nighttime in urban region (XJH and PD), which is consistent with the measured difference of  
509 | 12-14 ppbv. The observed daytime and nighttime O<sub>3</sub> concentrations at remote site DT show the  
510 | minimum difference of 5 ppbv which is also captured by WRF-Chem model due to the less impact  
511 | of anthropogenic emissions. In Fig. 8a, there exists a large O<sub>3</sub> plume with high concentration of  
512 | 40-48 ppbv in daytime in the west of Shanghai and its neighboring area from WRF-Chem  
513 | simulations. It is also illustrated by the daytime O<sub>3</sub> measurements at SS site with 40 ppbv.  
514 | However the daytime O<sub>3</sub> plume dissipates at night (Fig. 8b) leading to the significant difference  
515 | of O<sub>3</sub> concentration between day and night. Tie et al. (2013) suggested the enhancement of O<sub>3</sub>  
516 | concentration in the downwind of Shanghai due to the considerable O<sub>3</sub> formation in the aged  
517 | city plume transported westerly in September. According to the study of Tie et al. (2013), the O<sub>3</sub>  
518 | concentrations had a minimum within 20 km of the city, and enhanced at the west of 100-150  
519 | km away from the city in daytime, which was consistent with the results of daytime O<sub>3</sub>  
520 | distribution in Fig. 8a. It is shown in Fig. 8 thatIn addition, both model simulations and in-situ  
521 | measurements in daytime and nighttime highlight the lower O<sub>3</sub> concentration in urban zones  
522 | than that in suburb. The simulated daytime and nighttime O<sub>3</sub> concentration in downtown is  
523 | 22-24 28-32 ppbv and 12-14 ppbv respectively, significantly lower than that at sub-urban  
524 | (30-35 36-38 ppbv and 26-28 ppbv respectively) and rural area (40-42 40 ppbv and 36-38 ppbv  
525 | respectively), which is consistent with the measurements. Similarly, the measured daytime O<sub>3</sub>  
526 | concentration at downtown site XJH is 22-28 ppbv, lower than that at sub-urban site PD  
527 | and remote site DT by 12 ppbv and 26-21 ppbv respectively. Geng et al. (2007) suggested that under  
528 | VOC-limited regime, the lower O<sub>3</sub> concentration in downtown was resulted from the higher NO<sub>x</sub>  
529 | emission, which depressed the O<sub>3</sub> production process. Under high NO<sub>x</sub> conditions, the OH  
530 | radicals are lost by the reaction of NO<sub>2</sub> + OH → HNO<sub>3</sub> (Sillman, 1995). As a result, higher NO<sub>x</sub>  
531 | concentration in urban area leads to lower OH concentration, which results in smaller O<sub>3</sub>  
532 | production. Tang et al. (2008) also suggested that the O<sub>3</sub> concentration in Shanghai downtown  
533 | was higher on weekends than that on weekdays due to the reduced NO<sub>x</sub> concentration. However  
534 | the discrepancy is also evident between model results and measurements. For example, the  
535 | modeled nighttime O<sub>3</sub> concentrations at XJH and PD are about 2-3-6 ppbv higher-lower than the  
536 | measurements, perhaps due to the uncertainty of NO<sub>x</sub> and VOCs emission in urban area  
537 | suggested by Tie et al. (2009a). In addition, the calculated daytime O<sub>3</sub> concentrations in the  
538 | remote site DT and chemical site JS are lower than measurements by 8-10 and 6-5 ppbv  
539 | respectively. The former is resulted from the overestimation of the wind speed by WRF-Chem  
540 | model leading to excessive O<sub>3</sub> transport for underestimation (Zhou et al., 2017). While the latter  
541 | is mainly due to the prominent underestimation of the VOCs emission in the chemical zones  
542 | suggested by Tie et al. (2009a).

543

544 | **Figure 8.** The calculated distribution of (a) daytime and (b) nighttime O<sub>3</sub> concentration by  
545 | WRF-Chem (shade) in September of 2009 compared with measurements (circles) of 6 sites over  
546 | Shanghai. The minimum O<sub>3</sub> concentrations in daytime and nighttime both occur in urban center.

547

548 | Fig. 9a and b show the daily variations of O<sub>3</sub> and NO<sub>x</sub> concentrations compared between  
549 | WRF-Chem simulations and the in-situ measurements over 5 sites. The statistical analysis of  
550 | model performance for O<sub>3</sub> and NO<sub>x</sub> is listed in Table 1 and Table 2 respectively. The calculated  
551 | magnitude and daily variation of O<sub>3</sub> concentrations agree well with the measurements,

带格式的：下标

带格式的：下标

带格式的：下标

带格式的：下标

带格式的：下标

带格式的：下标

带格式的：下标

带格式的：下标

带格式的

---

552 suggesting that both meteorology and photochemistry are well reproduced by WRF-Chem model.  
553 For example, the Root Mean Square Error (RMSE) calculated between modeled and measured O<sub>3</sub>  
554 concentration are 7.4, 10.5, 12, 8.6, 9.2 ppbv for XJH, JS, DT, PD and BS respectively, and the  
555 difference between the simulation results and in-situ measurement is below 10%, which are very  
556 satisfactory compare with the similar works by Geng et al (2007) and Tie et al. (2013). The  
557 correlated coefficients (R) for the mean daily O<sub>3</sub> concentration range from 0.6 to 0.8 above 99%  
558 confidence over 5 sites, indicating good consistency of day by day variations between the model  
559 results and measurements. Comparably the O<sub>3</sub> concentration is best simulated by WRF-Chem at  
560 the downtown site XJH and sub-urban site PD with the lower RMSE and better R. However the  
561 discrepancy of daily O<sub>3</sub> concentration between the model and measurements is also evident. For  
562 example, a rapid change of O<sub>3</sub> concentration from 16 to 19 in September was observed over all  
563 sites, indicating it's a regional event instead of a local phenomenon. The O<sub>3</sub> concentration firstly  
564 increases significantly during 16-19 (episode-1), then sharply decreased during the later 4 days  
565 (episode-2). The similar rapid O<sub>3</sub> change in Shanghai was also reported by Tie et al. (2009a), and  
566 their explanation is that this episode was mainly related to the intensity of the sub-tropical  
567 high-pressure system on Pacific Ocean in summer. The model captures the O<sub>3</sub> variations and  
568 magnitudes during the both risen and fallen episodes very well at downtown site XJH, but  
569 substantially underestimates the increasing variability of O<sub>3</sub> concentration during episode-1 at  
570 sub-urban and rural sites by 10-15 ppbv. Geng et al. (2008a) suggested the "chemical transport of  
571 O<sub>3</sub>" from Shanghai downtown area to the distance of 18-36 km far away, which increased the O<sub>3</sub>  
572 concentration at sub-urban or rural sites. This "chemical transport of O<sub>3</sub>" is difficult to be  
573 reflected by WRF-Chem model due to the current inventory is too coarse to accurately reflect the  
574 detailed distribution and variation of NO<sub>x</sub> emission, e.g. the NO<sub>x</sub> emission from mobile source in  
575 the city. In addition, the underestimation of the O<sub>3</sub> concentration at suburb of Shanghai in  
576 summer is possibly attributed to the model bias of sea breeze simulations. Under the condition of  
577 weak sub-tropical pressure, the sea breeze develops at noontime to yield a cycling wind pattern  
578 in Shanghai, leading to the rapid accumulation of high O<sub>3</sub> concentration. The WRF-Chem usually  
579 underestimates the sea surface temperature, which tends to accelerate the sea breeze  
580 development and weak the O<sub>3</sub> trapping in the city (Tie et al., 2009a). The calculated daily NO<sub>x</sub>  
581 concentration by WRF-Chem compared with measurements are shown in Fig. 9b. Both the  
582 modeled and measured NO<sub>x</sub> concentrations at the remote site DT are very low, with the average  
583 of 1.4 and 2.9 ppbv respectively due to seldom anthropogenic emissions there. The calculated  
584 NO<sub>x</sub> concentration at XJH and PD are generally well consistent with the measurements with the  
585 excellent R of 0.8 and 0.82 and small RMSE of 6.9 and 7.5 ppbv respectively. However the NO<sub>x</sub>  
586 concentration is underestimated by WRF-Chem at sub-urban site BS in the steel zone. The  
587 calculated NO<sub>x</sub> concentration at BS is 16.1 ppbv, which is lower than the measurements by 5 ppbv.  
588 The difference of NO<sub>x</sub> concentrations between the model and observations is generally above  
589 10%, suggesting the performance of NO<sub>x</sub> simulation is somewhat lower than that of O<sub>3</sub>. It was  
590 also reported by Tie et al. (2007; 2009b; 2013), during the evaluation of the NO<sub>x</sub> calculations by  
591 WRF-Chem in MIRAGE-Shanghai and MIRAGE-mex campaign studies. The lifetime of NO<sub>x</sub> at the  
592 surface is about 1-2 days, shorter than O<sub>3</sub>. Thus the NO<sub>x</sub> concentration is determined by the  
593 detailed emissions and dynamical factors, which need to develop the advanced inventory with  
594 higher resolution to reproduce both the spatial distributions and temporal variations of NO<sub>x</sub>  
595 emission.

596

597 **Figure 9.** The calculated mean daily concentrations (ppbv) of (a) O<sub>3</sub> and (b) NO<sub>x</sub> at 5 sites in  
598 September of 2009 by WRF-Chem (red circles) and compared with measurements (blue circles).

599

#### 600 4.4 Sensitive study on the O<sub>3</sub> variability response to the emission change

601 The T1 experiment shows the excellent performance for O<sub>3</sub> and NO<sub>x</sub> simulations, including the  
602 spatial distribution pattern, and the day by day variation and magnitude. It is indicated that the  
603 emission in 2009 scenario used in WRF-Chem is reasonable, and the model is efficient for  
604 conducting the sensitive studies on O<sub>3</sub> variation response to the emission change. In order to  
605 better understand the measured long-term trend of O<sub>3</sub> concentration during the past ten years in  
606 Shanghai and its relationship to the emission reduction, several sensitive studies are conducted in  
607 this study (Table 3). The control study of T1 is conducted based on the NO<sub>x</sub> emission in 2009  
608 scenario in Shanghai. According to the study of Lin et al. (2017), the NO<sub>x</sub> emission in 2015 in  
609 Shanghai is reduced by 30% compared with that in 2009. Thus we conduct the sensitive  
610 experiment T2 by WRF-Chem, cutting the NO<sub>x</sub> emission by 30% compared with T1, whereas  
611 keeping the other emissions and meteorology same as T1. As a result, the calculated O<sub>3</sub>  
612 difference between T1 and T2 is likely attributed to the NO<sub>x</sub> emission reduction between 2015  
613 and 2009.

614 Fig. 10a shows the distribution of the difference of O<sub>3</sub> concentration simulated by T1 and T2  
615 (T2-T1). The reduction of NO<sub>x</sub> emission has the obvious effect on the magnitude and distribution  
616 of O<sub>3</sub> concentration. The O<sub>3</sub> concentration increases notably in urban area corresponding to the  
617 higher NO<sub>x</sub> emissions in Fig. 1, ranging from 2-7 ppbv. The enhancement of O<sub>3</sub> concentration is  
618 most significant in downtown and neighboring sub-urban zones, as well as the southern town,  
619 generally more than 4 ppbv. For example, the maximum increase in O<sub>3</sub> concentration is 6.4 ppbv  
620 occurred at downtown site XJH, followed by 4-5 ppbv at sub-urban site PD. The increasing rates  
621 of O<sub>3</sub> trend at XJH and PD are estimated at 1.06 ppbv yr<sup>-1</sup> and 0.96 ppbv yr<sup>-1</sup> from 2009 to 2015  
622 by WRF-Chem, which is consistent to the observed O<sub>3</sub> growth variability of 1-1.3 ppbv yr<sup>-1</sup>. The  
623 response of O<sub>3</sub> concentration to the NO<sub>x</sub> reduction is not evident in the rural area including the  
624 eastern part of Shanghai and the island with low NO<sub>x</sub> emissions. The comparison of T1 and T2  
625 further illustrates the speculation that the significant increasing trend of O<sub>3</sub> concentration during  
626 the past ten years in Shanghai is mostly attributed to the reduction of NO<sub>x</sub> emission as a result of  
627 the implementation of Shanghai Clean Air Action Plan.

628 The O<sub>3</sub> chemical formation is strongly related to NO<sub>x</sub> and VOCs concentrations. As discussed  
629 by Geng et al. (2008a) the O<sub>3</sub> chemical formation is clearly under VOC-limited regime in Shanghai  
630 and its neighboring area. Under the high NO<sub>x</sub> condition, NO tends to react with O<sub>3</sub> instead of NO<sub>2</sub>,  
631 flowing by NO<sub>2</sub> + OH → HNO<sub>3</sub>, causing the decrease of the reactivity and ensuing O<sub>3</sub>  
632 concentrations. Thus reduced NO<sub>x</sub> emission would result in increase in O<sub>3</sub> concentration, which  
633 has been discussed in Fig. 10a.

634 Despite of minor change of VOCs in the last ten years, it is worth to investigate the effect of  
635 the VOCs changes on O<sub>3</sub> concentrations in Shanghai. For this purpose, we conduct a sensitive  
636 study (T3), with 50% increase of VOCs emission compared with T1, but keeping NO<sub>x</sub> and other  
637 emissions as well as the meteorology same as T1. For RADM2 gas mechanism used in WRF-Chem,  
638 the VOCs are surrogated into 14 species, such as alkane, alkene, aromatic, formaldehyde, etc. All

---

639 the species of VOCs are increased by 50% at every model grid over Shanghai and at every hour.  
640 The difference of O<sub>3</sub> concentration between T3 and T1 (T3-T1) is shown in Fig. 10b. As we  
641 expected, the O<sub>3</sub> concentration in Shanghai is sensitive to the enhancement of VOCs emission,  
642 increased by 3-4 ppbv in urban area due to more NO is converted to NO<sub>2</sub> by reaction with RO<sub>2</sub>  
643 and HO<sub>2</sub>. Furthermore, the abundant O<sub>3</sub> plumes produced in the urban zones significantly  
644 transport to the downwind areas about 100-200 km away, resulting in elevated O<sub>3</sub> concentration  
645 in the western Shanghai by about 2 ppbv. According to Tie et al. (2013), the O<sub>3</sub> plume released in  
646 Shanghai urban area can be transported to downwind of the city by about 100-150 km away in  
647 the MIRAGE-shanghai field campaign. The model studies of T1, T2 and T3 highlight that under the  
648 emission of 2009 scenario, the O<sub>3</sub> chemical production is clearly under VOC-limit regime, either  
649 decreasing NO<sub>x</sub> concentration or increasing VOCs concentration would result in the O<sub>3</sub>  
650 enhancement. The analysis on in-situ measurements and model experiments jointly suggests that  
651 the significant O<sub>3</sub> increasing trend during the past ten years in Shanghai is mainly attributed to  
652 the large reduction of NO<sub>x</sub> emission.

653

654 **Figure 10.** The difference of O<sub>3</sub> concentration (ppbv) between (a) T2 and T1 (T2-T1), (b) T3 and  
655 T1 (T3-T1) respectively conducted by WRF-Chem model. The difference between T2 and T1 lies in  
656 the NO<sub>x</sub> emissions set in T2 (2015 scenario) is 30% lower than that in T1 (2009 scenario), which is  
657 estimated by Lin et al. (2017) according to the Shanghai Environment Yearbook. The difference  
658 between T3 and T1 is dependent on that the VOCs emission in T3 is 50% higher than that in T1.

659

#### 660 **4.5 The variation of O<sub>3</sub> production regime response to emission change**

661 The O<sub>3</sub> chemical mechanism in Shanghai was explored by several studies based on the in-situ  
662 measurements around 2008 and 2009. Geng et al. (2008a; 2008b), Ran et al. (2009) and Tie et al.  
663 (2009a) all revealed that the O<sub>3</sub> production around 2008 and 2009 in Shanghai was clearly under  
664 VOC-limit regime which was further illustrated by the above model studies. As indicated in Fig. 3,  
665 the significant decrease of NO<sub>x</sub> concentration is observed from 2009 to 2015 in Shanghai, while  
666 the VOCs concentration changed little during the same period. As we know, the O<sub>3</sub> chemical  
667 formation is strongly related to NO<sub>x</sub> and VOCs concentrations with nonlinearity. Thus the  
668 different variability of NO<sub>x</sub> and VOCs concentration from 2009 to 2015 inevitably has the large  
669 effect on the O<sub>3</sub> production regime, which need to be investigated deeply.

670 The complex relationship among NO<sub>x</sub>, VOCs and O<sub>3</sub> concentrations is usually depicted by O<sub>3</sub>  
671 isopleths diagram. The O<sub>3</sub> isopleths plot (Fig. 11) in Shanghai used in this study is constructed by  
672 the OZIPR model based on the in-situ measurements of O<sub>3</sub>, NO<sub>x</sub>, VOCs and meteorology. Under  
673 high VOCs and low NO<sub>x</sub> condition (low NO<sub>x</sub>/VOCs ratio), the O<sub>3</sub> production is not sensitive to  
674 VOCs, while positively correlated to NO<sub>x</sub> concentration, which is viewed as NO<sub>x</sub>-limited regime. By  
675 contrast, under low VOCs and high NO<sub>x</sub> condition (high NO<sub>x</sub>/VOCs ratio), the O<sub>3</sub> production tends  
676 to increase with the VOCs growth or NO<sub>x</sub> reduction, which is regarded as VOC-limited regime. The  
677 NO<sub>x</sub>-limited and VOC-limited regime is divided by a ridge line (the dot-dash line in Fig. 11) in the  
678 O<sub>3</sub> isopleths plot. The O<sub>3</sub> production is not sensitive to neither NO<sub>x</sub> concentration nor VOCs  
679 concentration when near the ridge line, which is regarded as the transition regime.

680 The O<sub>3</sub> chemical production regime at XJH and PD in 2009 and 2015 is positioned  
681 respectively in Fig. 11. In 2009 the O<sub>3</sub> production at both XJH and PD sites (marked as red and

---

682 blue hollow circle respectively) are clearly under VOC-limited regime. Thus decrease in NO<sub>x</sub>  
683 concentration leads to the O<sub>3</sub> enhancement, which is highlighted by the previous in-situ  
684 measurements and model experiments. Since then the O<sub>3</sub> production regime tends to move  
685 toward the dot-dash line due to the significant reduction of NO<sub>x</sub> concentration accompanied with  
686 the relative less change of VOCs at the two sites. In 2015 the O<sub>3</sub> production at XJH (marked as red  
687 solid circle) is still under VOC-limited regime, but for PD (marked as blue solid circle), it is close to  
688 the dot-dash line, approaching the transition regime between VOC-limited to NO<sub>x</sub>-limited. This  
689 result suggests that if the NO<sub>x</sub> emission keeps reduction after 2015 assuming the VOCs  
690 concentration keeps constant, the O<sub>3</sub> concentration will continue to increase at XJH, while at PD  
691 the O<sub>3</sub> concentration is supposed to be insensitive to the NO<sub>x</sub> change. According to the O<sub>3</sub>  
692 chemical regime depicted in Fig. 11, if the NO<sub>x</sub> concentration decreases by 5 ppbv after 2015, the  
693 peak O<sub>3</sub> concentration at XJH will further increase by 3 ppbv, whereas at PD it seems to change  
694 very slightly. To better understand this further change, more sensitive studies of WRF-Chem are  
695 conducted in the following sections.

696

697 **Figure 11.** The O<sub>3</sub> chemical production at downtown site XJH and sub-urban site PD in 2009 and  
698 2015 depicted by O<sub>3</sub> isopleths diagram. The hollow and solid red circles denote O<sub>3</sub> production  
699 regime at XJH in 2005 and 2019 respectively. The hollow and solid blue circles denote O<sub>3</sub>  
700 production regime at PD in 2005 and 2019 respectively

701

## 702 5 The future O<sub>3</sub> evaluation

### 703 5.1 The O<sub>3</sub> level in 2020

704 According to the Shanghai Clean Air Action Plan, the NO<sub>x</sub> emission in Shanghai will be further  
705 reduced by 20% in 2020 compared with that in 2015. According to the above analysis based on  
706 the O<sub>3</sub> isopleths plot (Fig. 11), the O<sub>3</sub> concentrations in downtown and sub-urban seem to have  
707 distinct different responses to further NO<sub>x</sub> reduction after 2015. In order to better understand  
708 the future O<sub>3</sub> variation, the sensitive experiment T4 is conducted by WRF-Chem with 20%  
709 reduction of NO<sub>x</sub> emission compared with T2. T2 and T4 represent the NO<sub>x</sub> emission in 2015 and  
710 2020 respectively. The other emissions and meteorology are set to be same as T1. The difference  
711 of O<sub>3</sub> concentration between T2 and T4 (T4-T2) is presented in Fig. 12a. The O<sub>3</sub> concentration  
712 keeps increasing in downtown area such as XJH site, ranging from 2-4 ppbv. However, for the  
713 sub-urban zones such as the PD site, the O<sub>3</sub> concentration changes very little response to the  
714 further NO<sub>x</sub> reduction, ranging from 0-1 ppbv. As discussed in Fig. 11, in 2015 the O<sub>3</sub> production  
715 at PD is possibly under the transition regime from VOC-limited to NO<sub>x</sub>-limited near the ridge line.  
716 As a result, the O<sub>3</sub> concentration is not sensitive to the variation of NO<sub>x</sub> concentration. However  
717 the O<sub>3</sub> concentration in the suburb zones generally decreases by 1ppbv, indicating that with the  
718 further NO<sub>x</sub> reduction after 2015 the O<sub>3</sub> chemical production transfers from VOCs-limited to  
719 NO<sub>x</sub>-limited regime in the rural of Shanghai.

720 It is suggested in Fig.11 that the O<sub>3</sub> production at downtown site XJH in 2015 is still under  
721 VOC-limited regime despite of the significant NO<sub>x</sub> reduction. The O<sub>3</sub> concentration would be also  
722 sensitive to the variation of VOCs concentration. Thus the sensitive experiment T5 is conducted  
723 by WRF-Chem model with 50% enhancement of VOCs emission compared with T2 (representing  
724 the emission in 2015 scenario). It is presented in Fig. 12b that the O<sub>3</sub> concentration increases by

---

725 2-3 ppbv in downtown area due to the enhancement of VOCs, suggesting that the O<sub>3</sub> production  
726 at downtown in 2015 is still under VOC-limited regime, which is consistent with the results in Fig.  
727 11. Moreover the O<sub>3</sub> plumes produced in urban area transport to the downwind area to  
728 accumulate the high O<sub>3</sub> concentration in the western area to Shanghai by 2 ppbv. While at  
729 sub-urban site PD, the O<sub>3</sub> concentration changes less than 1 ppbv response to the increase in  
730 VOCs emission, which is similar as the very weak O<sub>3</sub> variations relative to the NO<sub>x</sub> reduction in Fig.  
731 12a. Overall, the models studies of T4 and T5 jointly suggest that the O<sub>3</sub> concentration at  
732 sub-urban site PD in 2015 is not sensitive to either NO<sub>x</sub> or VOCs variations due to the O<sub>3</sub>  
733 production is under the transition regime depicted in the O<sub>3</sub> isopleths plot.

734

735 **Figure 12.** The difference of O<sub>3</sub> concentration (ppbv) between (a) T4 and T2 (T4-T2), (b) T5 and  
736 T2 (T5-T2) respectively conducted by WRF-Chem model. The difference between T4 and T2 is  
737 that the NO<sub>x</sub> emissions set in T4 (2020 scenario) is 20% lower than that in T2 (2015 scenario),  
738 which is estimated according to the Shanghai Clean Air Action Plan. The difference between T5  
739 and T2 lies in that the VOCs emission in T5 is 50% higher than that in T2.

740

## 741 5.2 The O<sub>3</sub> chemical production after 2020

742 The above study shows that the O<sub>3</sub> production at sub-urban site PD in 2020 will likely transfer  
743 from VOCs-limited regime to NO<sub>x</sub>-limited regime without consideration of possible VOCs changes.  
744 For the purpose of the O<sub>3</sub> pollution control strategy, it is worth to estimate the O<sub>3</sub> level response  
745 to emission change after 2020 in Shanghai. It is also essential to access how many NO<sub>x</sub> emission  
746 need to be cut after 2020 will cease the O<sub>3</sub> enhancement in downtown area. Thus the sensitive  
747 experiment T6 is conducted by further 20% reduction of NO<sub>x</sub> emission from 2020 scenario (T4).  
748 The difference of O<sub>3</sub> concentration between T6 and T4 (T6-T4) is shown in Fig. 13a. It is clear that  
749 the O<sub>3</sub> concentration at downtown keeps nearly constant regardless of the further reduction of  
750 NO<sub>x</sub> emission after 2020. That is to say the increasing trend of O<sub>3</sub> in downtown with the NO<sub>x</sub>  
751 reduction ceases after 2020, indicating that the O<sub>3</sub> production likely approaches the transition  
752 regime. In addition, the O<sub>3</sub> concentration decreases significantly out of the downtown area,  
753 ranging from 2-3 ppbv in sub-urban zones, and more than 4 ppbv in suburb, indicating that the  
754 O<sub>3</sub> production in Shanghai transfers to NO<sub>x</sub>-limited regime after 2020 except the downtown area  
755 where the O<sub>3</sub> production is likely near the transition zone. On the other hand, if the NO<sub>x</sub> emission  
756 is kept constant after 2020 as T4, while the VOCs emission is increased by 50% conducted in T7  
757 experiment, the O<sub>3</sub> concentration (Fig. 13b) changes little in both urban and suburb area in  
758 Shanghai which is different from the previous model study of T5 the T3 when O<sub>3</sub> production is  
759 under VOC-limited condition. It is suggested that the O<sub>3</sub> concentration after 2020 is not sensitive  
760 to the variation of VOCs concentration because the continuous reduction of NO<sub>x</sub> emission keeps  
761 in promoting the O<sub>3</sub> production to transfer into NO<sub>x</sub>-limited regime. Thus further reduction of  
762 NO<sub>x</sub> tends to decrease the O<sub>3</sub> concentration in Shanghai.

763

764 **Figure 13.** The difference of O<sub>3</sub> concentration (ppbv) between (a) T6 and T4 (T6-T4), (b) T7 and  
765 T4 (T7-T4) respectively conducted by WRF-Chem model. The NO<sub>x</sub> emissions set in T6 is 20% lower  
766 than that in T4 (2020 scenario). The VOCs emission in T7 is 50% higher than that in T4.

767

---

768 **Conclusions**

769 O<sub>3</sub> pollution is a serious issue in China. Better understanding the elevated O<sub>3</sub> and its response to  
770 emission change is important for Chinese megacities. In this study, we analyze the increasing  
771 trend of O<sub>3</sub> concentration by long-term measurements of O<sub>3</sub> and its precursors as well as  
772 meteorology in Shanghai combined with the WRF-Chem model. The O<sub>3</sub> production regime  
773 response to the emission change in Shanghai during the past ten years is also explored by O<sub>3</sub>  
774 isopleths plot. In addition, the future O<sub>3</sub> variation and its chemical production in Shanghai are  
775 evaluated by WRF-Chem model. The main conclusions are summarized as follows:

776 (1) The daily maximum O<sub>3</sub> concentration measured in Shanghai increased significantly from  
777 2006 to 2015 with the rate of 0.808 ppbv yr<sup>-1</sup> at downtown site XJH and 1.374 ppbv yr<sup>-1</sup> at  
778 sub-urban site PD respectively. The observed increasing trend of O<sub>3</sub> is not limited in the urban  
779 zones but expanded to the larger scale covering the total Shanghai city. The NO<sub>x</sub> and VOCs  
780 concentrations presented different variability from O<sub>3</sub> during the same period, in which NO<sub>x</sub>  
781 concentration decreases significantly at both XJH and PD sites, whereas the VOCs changes very  
782 little without evident trend.

783 (2) Because there are minor trends of measured O<sub>3</sub> photolysis, local dispersion and regional  
784 transport resulted from meteorology, it is speculated that the significant O<sub>3</sub> increasing trend  
785 during 2006 to 2015 in Shanghai is likely attributed to the reduction of NO<sub>x</sub> concentration as a  
786 result of the strong VOCs-limited regime for O<sub>3</sub> production. The nighttime O<sub>3</sub> is more sensitive to  
787 NO<sub>x</sub> reduction than that in daytime, because of more O<sub>3</sub> is depressed by NO<sub>x</sub> in nighttime. As a  
788 result, the observed nighttime O<sub>3</sub> concentration at XJH increases more rapidly than that in  
789 daytime response to the NO<sub>x</sub> reduction.

790 (3) The WRF-Chem model is utilized to calculate the long term O<sub>3</sub> variations response to  
791 emission change. The sensitive experiments illustrate that either reduction of NO<sub>x</sub> emission or  
792 growth of VOCs emission conducted by WRF-Chem lead to the significant enhancement in O<sub>3</sub>  
793 concentration in urban zones in 2009 as the baseline, indicating the O<sub>3</sub> production is clearly  
794 under VOC-limited regime. The calculated O<sub>3</sub> concentration increases by 1-7 ppbv in urban zones  
795 from 2009 to 2015 resulted from 30% reduction of NO<sub>x</sub> emission estimated by Shanghai  
796 Environmental Monitoring Center. The enhancement of O<sub>3</sub> concentration is significant in urban  
797 zones generally more than 4 ppbv, with the maximum elevation of 6-7 ppbv occurred at  
798 downtown area, which is consistent with the measurements. The increasing rates of O<sub>3</sub> trend at  
799 downtown site XJH and sub-urban site PD are estimated at 1.06 ppbv yr<sup>-1</sup> and 0.96 ppbv yr<sup>-1</sup> from  
800 2009 to 2015 by WRF-Chem, which is close to the observed O<sub>3</sub> growth variability of 1-1.3 ppbv  
801 yr<sup>-1</sup>. This result suggests that the observed increasing trend of O<sub>3</sub> concentration during the past  
802 ten years in Shanghai is likely attributed to the reduction of NO<sub>x</sub> emission under the VOC-limited  
803 condition for O<sub>3</sub> production.

804 (4) The model sensitive study suggests that significant decrease in NO<sub>x</sub> concentration  
805 combined with the obscure VOCs variation from 2006 to 2015 gradually promotes the O<sub>3</sub>  
806 chemical production in Shanghai from VOC-limited to NO<sub>x</sub>-limited, which is consistent with the O<sub>3</sub>  
807 isopleths diagram. The O<sub>3</sub> isopleths plot shows that O<sub>3</sub> production is in VOC-limited regime in  
808 both downtown site XJH and sub-urban site PD in 2009. With the 30% reduction of NO<sub>x</sub> emission  
809 from 2009 to 2015 estimated by Shanghai Environmental Monitoring Center, the O<sub>3</sub> production in  
810 XJH is still under VOC-limited regime, while the O<sub>3</sub> production moves to the transition regime in  
811 PD, suggesting that the O<sub>3</sub> concentration in sub-urban zones is not sensitive to the variation of

---

812 either NO<sub>x</sub> or VOCs concentration.

813 (5) In order to better understand the O<sub>3</sub> control strategy in Shanghai, the future O<sub>3</sub>  
814 production is estimated by WRF-Chem. The O<sub>3</sub> concentration in Shanghai downtown would keep  
815 increasing till 2020 with the 20% reduction of NO<sub>x</sub> emission after 2015 estimated by Shanghai  
816 Clean Air Action Plan. If the NO<sub>x</sub> emission is further decreased by 20% after 2020, The O<sub>3</sub>  
817 concentration will decrease by 2-3 ppbv in sub-urban zones, and more than 4 ppbv in suburb.  
818 While the O<sub>3</sub> concentration in downtown is not sensitive to either NO<sub>x</sub> reduction or VOCs  
819 enhancement after 2020, indicating the O<sub>3</sub> production in shanghai will transfer to NO<sub>x</sub>-limited  
820 regimes except downtown where the O<sub>3</sub> production is likely close to the transition regime.  
821 Further reduction of NO<sub>x</sub> emission after 2020 tend to mitigate the O<sub>3</sub> pollution in Shanghai.

822 (6) There are some uncertainties and limitations existed in the study. First, the  
823 inhomogeneity of the NO<sub>x</sub> reduction is not considered in the sensitive experiments by lacking of  
824 the high resolution emission inventory (e.g. 1 km resolution). Second, the variation of VOCs  
825 emission is not taken into account in the model experiments due to the more uncertainties  
826 existed in the current VOCs emission inventory. While O<sub>3</sub> production in Shanghai is very sensitive  
827 to some VOC species, especially aromatics. Thus the accurate emission inventory of VOCs need to  
828 be developed and included in the future study. Third, the same meteorology is used for all  
829 WRF-Chem simulations. However the O<sub>3</sub> photolysis, advection, and vertical diffusion are all  
830 strongly affected by meteorology. The change of meteorology would be considered and  
831 evaluated in the future studies for more deep investigation.

832

833 **Data availability.** The data used in this paper can be provided upon request from Jianming Xu  
834 (metxujm@163.com).

835

836 **Author contributions.** XT came up with the original idea of investigating the impact of emission  
837 change on long term O<sub>3</sub> variations by. XT and JX designed the analysis method. JX conducted the  
838 analysis. WG, YL and QF provided the observational data and helped in discussion.

839

840 **Competing interests.** The authors declare that they have no conflict of interest.

841

842 **Acknowledgements.** This study was funded by the National Key R&D Program of China (grant  
843 2018YFC0213800), the National Natural Science Foundation of China (91644223, 41430424 and  
844 41730108).

845



---

846 **References**

- 847 Binkowski, F. S. and Roselle, S. J.: Models-3 community multi scale air quality (CMAQ) model  
848 aerosol component – 1. Model description, *Journal of Geophysical Research*, 108 (D6),  
849 4183, doi:10.1029/2001jd001409, 2003.
- 850 Brasseur, G. P., Orlando, J. J., and Tyndall, G. S.: *Atmospheric chemistry and global change*, Oxford  
851 University Press, Cambridge, USA, 654 pp., 1999.
- 852 Cai, C. J., Geng, F. H., Tie, X. X., Yu, Q., and An J. L.: Characteristics and source apportionment of  
853 VOCs measured in Shanghai, China, *Atmospheric Environment*, 44, 5005-5014, 2010.
- 854 Chen, F. and Dudhia, J.: Coupling an advanced land surface hydrology model with the Penn  
855 State-NCAR MM5 modeling system, Part I: Model implementation and sensitivity, *Monthly*  
856 *Weather Review*, 129, 569–585, 2001.
- 857 Dudhia, J.: Numerical study of convection observed during the winter monsoon experiment using  
858 a mesoscale two-dimensional model, *Journal of the Atmospheric Sciences*, 46, 3077–3107,  
859 1989.
- 860 Emmons, L. K., Walters, S., Hess, P. G., Lamarque, J. F., Pfister, G. G., Fillmore, D., Granier, C.,  
861 Aguenther, A., Kinnison, D., Laepple, T., Orlando, J., Tie, X., Tyndall, G., Wiedinmyer, C.,  
862 Baughcum, S. L., and Kloster, S.: Description and evaluation of the model for ozone and  
863 related chemical tracers, version4 (MOZART-4), *Geoscientific Model Development*, 3, 43–67,  
864 2010.
- 865 Gao, W., Tie, X. X., Xu, J. M., Huang, R. J., Mao, X. Q., Zhou, G. Q., and Chang, L. Y.: Long-term  
866 trend of O<sub>3</sub> in a mega City (Shanghai), China: Characteristics, causes, and interactions with  
867 precursors, *Science of the Total Environment*, 603-604, 425-433, 2017.
- 868 Geng, F. H., Zhao, C. S., Tang, X., Lu, G. L., and Tie, X. X.: Analysis of ozone and VOCs measured in  
869 Shanghai: a case study, *Atmospheric Environment*, 41, 989–1001, 2007.
- 870 Geng, F. H., Tie, X., Xu, J., Zhou, G., Peng, L., Gao, W., Tang, X., Zhao, C.: Characterizations of ozone,  
871 NO<sub>x</sub>, and VOCs measured in Shanghai, China, *Atmospheric Environment*, 42, 6873–6883,  
872 2008a.
- 873 Geng, F. H., Zhang, Q., Tie, X., Huang, M., Ma, X., Deng, Z., Quan, J., and Zhao, C.: Aircraft  
874 measurements of O<sub>3</sub>, NO<sub>x</sub>, CO, VOCs, and SO<sub>2</sub> in the Yangtze River Delta region, *Atmospheric*  
875 *Environment*, 43, 584–593, 2008b.
- 876 Geng, F. H., Tie, X., Guenther, A., Li, G., Cao, J., and Harley, P.: Effect of isoprene emissions from  
877 major forests on ozone formation in the city of Shanghai, China, *Atmospheric Chemistry and*  
878 *Physics*, 11, 10449–10459, 2011.
- 879 Geng, F. H., Mao, X. Q., Zhou, M. Y., Zhong, S. Y., and Lenschow, D.: Multi-year ozone  
880 concentration and its spectra in Shanghai, China, *Science of the Total Environment*, 521-522,  
881 135-143, 2015.
- 882 Gery, M. W., and Crouse, R. R.: *User’s Guide for Executing OZIPR*, Atmospheric Research and  
883 Exposure Assessment Lab., Office of Research and Development, U.S. EPA, Research Triangle  
884 Park, N. C., <http://www.epa.gov/scram001/models/other/oziprdme.txt>, 2002.
- 885 Grell, G. A., Peckham, S. E., Schmitz, R., McKeen, S. A., Frost, G., Skamarock, W. C., and Eder, B.:  
886 Fully coupled “online” chemistry within the WRF model, *Atmospheric Environment*, 39,  
887 6957–6975, 2005.
- 888 Guenther, A., Karl, T., Harley, P., Wiedinmyer, C., Palmer, P. I., and Geron, C.: Estimates of global  
889 terrestrial isoprene emissions using MEGAN (Model of Emissions of Gases and Aerosols from

---

890 Nature), *Atmospheric Chemistry and Physics*, 6, 3181–3210, 2006.

891 Hong, S. Y. and Lim, J. O. J.: The WRF Single-Moment 6-Class Microphysics Scheme (WSM6),  
892 *Journal of the Korean Meteorological Society*, 42, 129–151, 2006.

893 Hu, X. M., Klein, P. M., and Xue, M.: Evaluation of the updated YSU planetary boundary layer  
894 scheme within WRF for wind resource and air quality assessments, *Journal of Geophysical*  
895 *Research-Atmospheres*, 118, 10490-10505, 2013.

896 Hu, X. M., Xue, M., Klein, P. M., Illston, B. G., and Chen, S.: Analysis of Urban Effects in Oklahoma  
897 City using a Dense Surface Observing Network, *Journal of Applied Meteorology and*  
898 *Climatology*, 55, 723-741, 2016.

899 Lei, W., Foy, B. de, Zavala, M., Volkamer, R., and Molina, L. T.: Characterizing ozone production in  
900 the Mexico City Metropolitan Area: a case study using a chemical transport model,  
901 *Atmospheric Chemistry and Physics*, 7, 1347-1366, 2007.

902 Li, G., Lei, W., Zavala, M., Volkamer, R., Dusanter, S., Stevens, P., and Molina, L. T.: Impacts of  
903 HONO sources on the photochemistry in Mexico City during the MCMA-2006/MILAGO  
904 Campaign, *Atmospheric Chemistry and Physics*, 10, 6551–6567, 2010.

905 Li, G., Bei, N., Tie, X., and Molina, L. T.: Aerosol effects on the photochemistry in Mexico City  
906 during MCMA-2006/MILAGRO campaign, *Atmospheric Chemistry and Physics*, 11,  
907 5169–5182, 2011.

908 Li, K., Jacob, D. J., Liao, H., Shen, L., Zhang, Q., and Bates, K. H.: Anthropogenic drivers of  
909 2013-2017 trends in summer surface ozone in China, *PANS*, 116, 2, 422-427, 2019.

910 Lin, X., Trainer, M., and Liu, S. C.: On the nonlinearity of the tropospheric ozone production,  
911 *Journal of Geophysical Research Atmospheres*, 93 (D12), 15879–15888, 1988.

912 Lin, Y. F., Wang, Q., Fu, Q. Y., Duan, Y. S., Xu, J. M., Liu, Q. Z., Li, F., and Huang, K.: Temporal-spatial  
913 characteristics and impact factors of ozone pollution in Shanghai, *Environmental Monitoring*  
914 *in China (in Chinese)*, 33, 4, 60-67, 2017.

915 Lin, Y. L., Farley, R. D., and Orville, H. D.: Bulk parameterization of the snowfield in a cloud model,  
916 *Journal of Climate and Applied Meteorology*, 22, 1065–1092, 1983.

917 Lu, X., Hong, J., Zhang, L., Cooper, O., Schultz, M., Xu, X., Wang, T., Gao, M., Zhao, Y., and Zhang, Y.:  
918 Severe surface ozone pollution in China: A global perspective, *Environmental Science*  
919 *&Technology Letters*, 5, 487–494, 2018.

920 Monks, P. S., Archibald, A. T., Colette, A., Cooper, O., Coyle, M., Derwent, R., Fowler, D., Granier, C.,  
921 Law, K. S., Mills, G. E., Stevenson, D. S., Tarasova, O., Thouret, V., von Schneidemesser, E.,  
922 Sommariva, R., Wild, O., and Williams, M. L.: Tropospheric ozone and its precursors from the  
923 urban to the global scale from air quality to short-lived climate forcer, *Atmospheric*  
924 *Chemistry and Physics*, 15, 8889–8973, 2015.

925 Ma, Z., Xu, J., Quan, W., Zhang, Z., Lin, W., and Xu, X.: Significant increase of surface ozone at a  
926 rural site, north of eastern China, *Atmospheric Chemistry and Physics*, 16, 3969–3977, 2016.

927 Nenes, A., Pandis, S. N., and Pilinis, C.: ISORROPIA: A new thermodynamic equilibrium model for  
928 multiphase multicomponent inorganic aerosols, *Aquatic Geochemistry*, 4, 123–152, 1998.

929 Ran, L., Zhao, C., Geng, F., Tie, X., Tang, X., Peng, L., Zhou, G., Yu, Q., Xu, J., and Guenther, A.:  
930 Ozone photochemical production in urban Shanghai, China: analysis based on ground level  
931 observations, *Journal of Geophysical Research Atmospheres*, 114, D15301, 2009.

932 Sillman, S.: The use of NO<sub>y</sub>, H<sub>2</sub>O<sub>2</sub>, and HNO<sub>3</sub> as indicators for ozone-NO<sub>x</sub>-hydrocarbon sensitivity  
933 in urban locations, *Journal of Geophysical Research Atmospheres*, 100, 14175–14188, 1995.

---

934 Sillman, S.: The relation between ozone, NO<sub>x</sub> and hydrocarbons in urban and polluted rural  
935 environments, *Atmospheric Environment*, 33, 1821–1845, 1999.

936 Song, J., Lei, W., Bai, N., Zavala, M., de Foy, B., Volkamer, R., Cardenas, B., Zheng, J., Zhang, R., and  
937 Molina L. T.: Ozone response to emission changes: a modeling study during the  
938 MCMA-2006/MILAGRO Campaign, *Atmospheric Chemistry and Physics*, 10, 3827–3846, 2010

939 Stockwell, W. R., Middleton, P., Chang, J. S., and Tang, X.: The second generation regional acid  
940 deposition model chemical mechanism for regional air quality modeling, *Journal of*  
941 *Geophysical Research Atmospheres*, 95, 16343–16367, 1990.

942 Sun, L., Xue, L., Wang, T., Gao, J., Ding, A., Copper, O., Lin, M., Xu, P., Wang, Z., Wang, X., Wen, L.,  
943 Zhu, Y., Chen, T., Yang, L., Wang, Y., Chen, J., and Wang, W.: Significant increase of  
944 summertime ozone at Mount Tai in central eastern China, *Atmospheric Chemistry and*  
945 *Physics*, 16, 10637–10650, 2016.

946 Tai, A. P. K., Martin, M. V., and Heald, C. L.: Threat to future global food security from climate  
947 change and ozone air pollution, *Nature Climate Chang*, 4, 817–821, 2014.

948 Tang, G., Li, X., Wang, Y., Xin, J., and Ren, X.: Surface ozone trend details and interpretations in  
949 Beijing, 2001–2006, *Atmospheric Chemistry and Physics*, 9, 8813–8823, 2009.

950 Tang, W. Y., Zhao, C. S., Geng, F. H., Peng, L., Zhou, G. Q., Gao, W., Xu, J. M., and Tie, X. X.: Study of  
951 ozone "weekend effect" in Shanghai, *Science in China Series D: Earth Sciences*, 51, 9,  
952 1354–1360, 2008.

953 Tie, X., Brasseur, G., Emmons, L., Horowitz, I., and Kinnison, D.: Effects of aerosols on  
954 tropospheric oxidants: a global model study, *Journal of Geophysical Research Atmospheres*,  
955 106, 22931–22964, 2001.

956 Tie, X., Madronich, S., Walters, S., Zhang, R. Y., Rasch, P., and Collins, W.: Effect of clouds on  
957 photolysis and oxidants in the troposphere, *Journal of Geophysical Research Atmospheres*,  
958 108, 4642, doi:10.1029/2003jd003659, 2003.

959 Tie, X., Madronich, S., Li, G., Ying, Z., Zhang, R., Garcia, A., Taylor, J., and Liu, Y.: Characterizations  
960 of chemical oxidants in Mexico City: A regional chemical dynamical model (WRF-Chem)  
961 study, *Atmospheric Environment*, 41, 1989–2008, 2007.

962 Tie, X., Geng, F. H., Peng, L., Gao, W., Zhao, C. S.: Measurement and modeling of O<sub>3</sub> variability in  
963 Shanghai, China: application of the WRF-Chem model, *Atmospheric Environment*, 43,  
964 4289–4302, 2009a.

965 Tie, X., Madronich, S., Li, G., Ying, Z., Weinheimer, A., Apel, E., and Campos, T.: Simulation of  
966 Mexico City plumes during the MIRAGE-Mex field campaign using the WRF-Chem model,  
967 *Atmospheric Chemistry and Physics*, 9, 4621–4638, 2009b.

968 Tie, X., Geng, F., Guenther, A., Cao, J., Greenberg, J., Zhang, R., Apel, E., Li, G., Weinheimer, A.,  
969 Chen, J., and Cai, C.: Megacity impacts on regional ozone formation: observations and  
970 WRF-Chem modeling for the MIRAGE-Shanghai field campaign, *Atmospheric Chemistry and*  
971 *Physics*, 13, 5655–5669, doi:10.5194/acp-13-5655-2013, 2013.

972 Wang, H. J., and Chen, H. P.: Understanding the recent trend of haze pollution in eastern China:  
973 roles of climate change, *Atmospheric Chemistry and Physics*, 16, 4205–4211, 2016

974 Wang, T., Xue, L., Brimblecombe, P., Lam Y. F., Li, L., and Zhang, L.: Ozone pollution in China: A  
975 review of concentrations, meteorological influences, chemical precursors, and effects,  
976 *Science of Total Environment*, 575, 1582–1596, 2017.

977 Wesely, M. L.: Parameterization of surface resistances to gaseous dry deposition in regional-scale

---

978 numerical models, *Atmospheric Environment*, 23, 1293–1304, 1989.

979 Xu, J. M., Yan, F. X., Xie, Y., Wang, F. Y., Wu, J. B., and Fu, Q. Y.: Impact of meteorological conditions  
980 on a nine-day particulate matter pollution event observed in December 2013, Shanghai,  
981 China, *Particuology*, 20, 69–79, 2015.

982 Xu, J. M., Chang, L. Y., Yan, F. X., and He, J. H.: Role of climate anomalies on decadal variation in  
983 the occurrence of wintertime haze in the Yangtze River Delta, China, *Science of the Total  
984 Environment*, 599-600, 918-925, 2017.

985 Ying, Z. M., Tie, X., and Li, G. H.: Sensitivity of ozone concentrations to diurnal variations of  
986 surface emissions in Mexico City: A WRF/Chem modeling study, *Atmospheric Environment*,  
987 43, 851–859, 2009.

988 Zhang, Q., Streets, D. G., Carmichael, G. R., He, K. B., Huo, H., Kannari, A., Klimont, Z., Park, I. S.,  
989 Reddy, S., Fu, J. S., Chen, D., Duan, L., Lei, Y., Wang, L. T., Yao, Z. L.: Asian emissions in 2006  
990 for the NASA INTEX-B mission, *Atmospheric Chemistry and Physics*, 9, 5131-5153, 2009.

991 Zhao, S., Li, J. P., Sun, C.: Decadal variability in the occurrence of wintertime haze in central  
992 eastern China tied to the Pacific decadal oscillation, *Scientific Reports*, 6, 27424, 2016.

993 Zheng, B., Tong, D., Li, M., Liu, F., Hong, C., Geng, G., Li, H., Li, X., Peng, L., Qi, J., Yan, L., Zhang, Y.,  
994 Zhao, H., Zheng, Y., He, K., and Zhang, Q.: Trends in China's anthropogenic emissions since  
995 2010 as the consequence of clean air actions, *Atmospheric Chemistry and Physics*, 18,  
996 14095-14111, <https://doi.org/10.5194/acp-18-14095-2018>, 2018.

997 Zhou, G. Q., Xu, J. M., Xie, Y., Chang, L. Y., and Gao, W.: Numerical air quality forecasting over  
998 eastern China: An operational application of WRF-Chem, *Atmospheric Environment*, 153,  
999 94-108, 2017.

1000

1001 **Table 1.** Statistical analysis on O<sub>3</sub> simulation in September of 2009 by WRF-Chem model  
 1002 compared with measurements of 5 sites (XJH, JS, DT, PD, BS) over Shanghai. MO and MM  
 1003 represent the mean value (unit: ppbv) of observed and modeled O<sub>3</sub> concentration respectively.  
 1004 RMSE and R are the Root Mean Square Error and correlated coefficient respectively calculated  
 1005 between modeled and measured O<sub>3</sub> concentration.  
 1006

	MO	MM	RMSE	R (99% confidence)
		ppbv		\
<b>XJH</b>	21.6	23.0	7.2	0.78
<b>JS</b>	34.6	30.0	10.3	0.64
<b>DT</b>	47.3	40.3	12.0	0.61
<b>PD</b>	33.5	34.9	8.6	0.74
<b>BS</b>	31.7	31.2	9.3	0.67

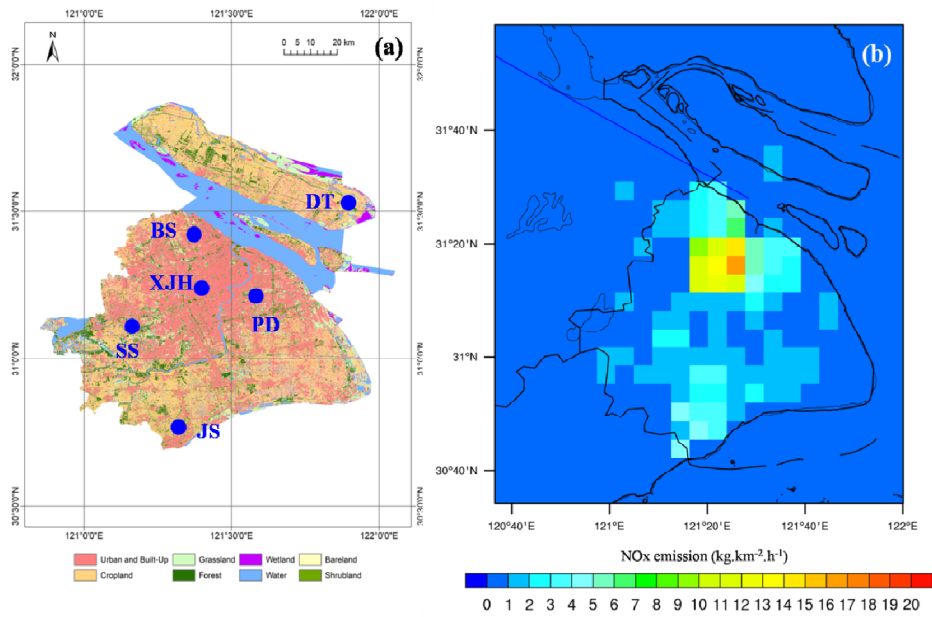
1007  
 1008  
 1009 **Table 2.** Statistical analysis on NO<sub>x</sub> simulation in September of 2009 by WRF-Chem model  
 1010 compared with measurements of 5 sites (XJH, JS, DT, PD, BS) over Shanghai. MO and MM  
 1011 represent the mean value (unit: ppbv) of observed and modeled NO<sub>x</sub> concentration respectively.  
 1012 RMSE and R are the Root Mean Square Error and correlated coefficient respectively calculated  
 1013 between modeled and measured NO<sub>x</sub> concentration.  
 1014

	MO	MM	RMSE	R (99% confidence)
		ppbv		\
<b>XJH</b>	32.1	33.7	7.0	0.74
<b>JS</b>	14.9	14.7	7.6	0.61
<b>DT</b>	3.0	1.5	2.3	0.6
<b>PD</b>	20.3	16.8	7.5	0.82
<b>BS</b>	21.6	16.1	9.8	0.8

1015  
 1016  
 1017 **Table 3.** Scheme of WRF-Chem sensitivity simulations.  
 1018

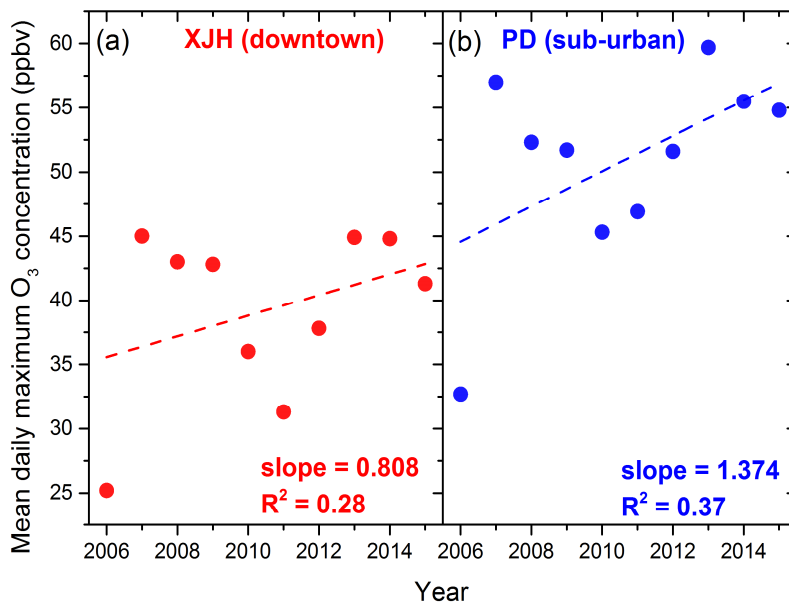
Simulation	NO <sub>x</sub> EI	VOCs EI	Meteorology
<b>T1 (Control Run)</b>	2009	2009	September of 2009
<b>T2</b>	2015 (30% reduction)	2009	September of 2009
<b>T3</b>	2009	50% increasing	September of 2009
<b>T4</b>	2020 (50% reduction)	2009	September of 2009
<b>T5</b>	2015	50% increasing	September of 2009
<b>T6</b>	70% reduction	2009	September of 2009
<b>T7</b>	2020 (50% reduction)	50% increasing	September of 2009

1019  
 1020  
 1021  
 1022

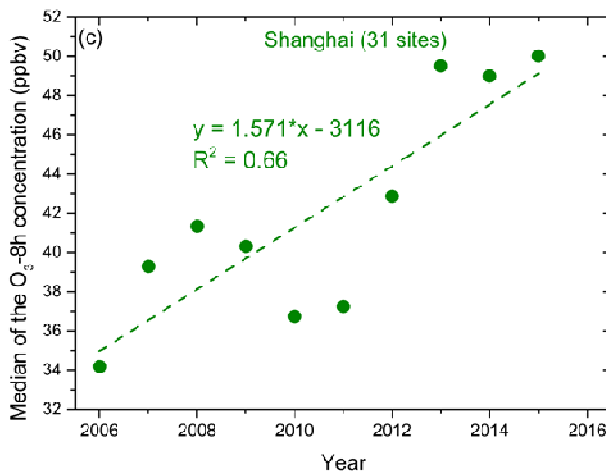


1023  
 1024  
 1025  
 1026

**Figure1** (a) The distribution of land-use category in Shanghai. The blue dots denote the locations of 6 sties (XJH, BS, PD, SS, JS, DT). (b) The NOx emission of 2009 scenario in Shanghai.

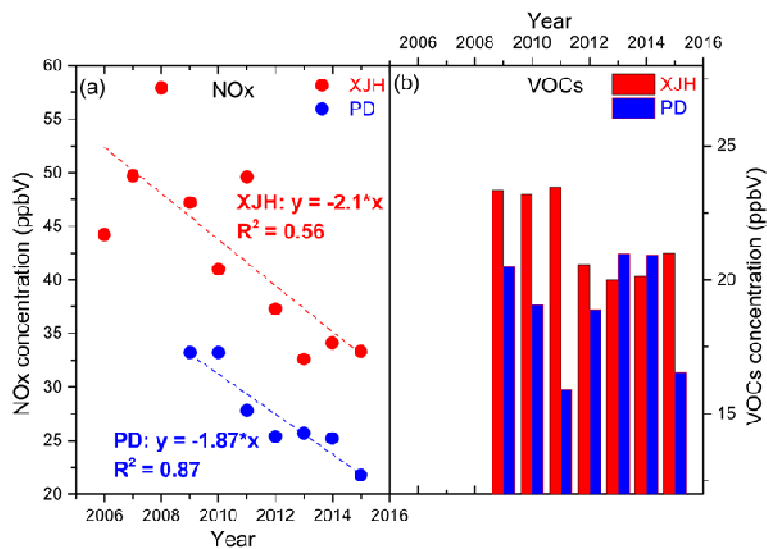


1027



1028

1029 **Figure 2.** The annual variation of daily maximum O<sub>3</sub> concentration (ppbv) from 2006 to 2015 at (a)  
 1030 downtown site XJH and (b) sub-urban site PD, both presenting the significant increasing trends  
 1031 with 0.808 ppbv yr<sup>-1</sup> at XJH and 1.374 ppbv yr<sup>-1</sup> at PD. The variation of the median 8-h O<sub>3</sub>  
 1032 concentration (ppbv) from 2006 to 2015 averaged for 31 sites over Shanghai (c), also shows the  
 1033 increasing variability of 1.571 ppbv yr<sup>-1</sup>.

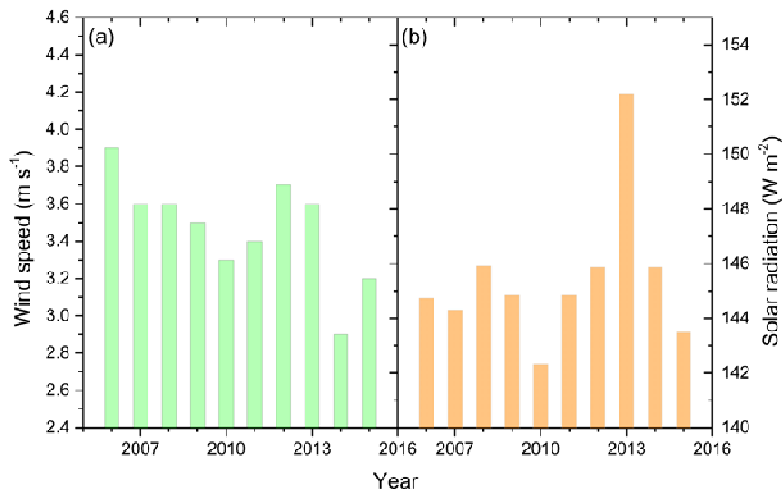


1034

1035 **Figure 3.** The mean annual concentrations (ppbv) of (a) NO<sub>x</sub> (dots) and (b) VOCs (bars) from 2006  
 1036 to 2015 at downtown site XJH and sub-urban site PD respectively. The NO<sub>x</sub> concentrations at XJH  
 1037 and PD both present obvious decreasing trends with 2.1 ppbv yr<sup>-1</sup> and 1.87 ppbv yr<sup>-1</sup>. While the  
 1038 VOCs concentrations at both sites present no clear inter-annual trends.

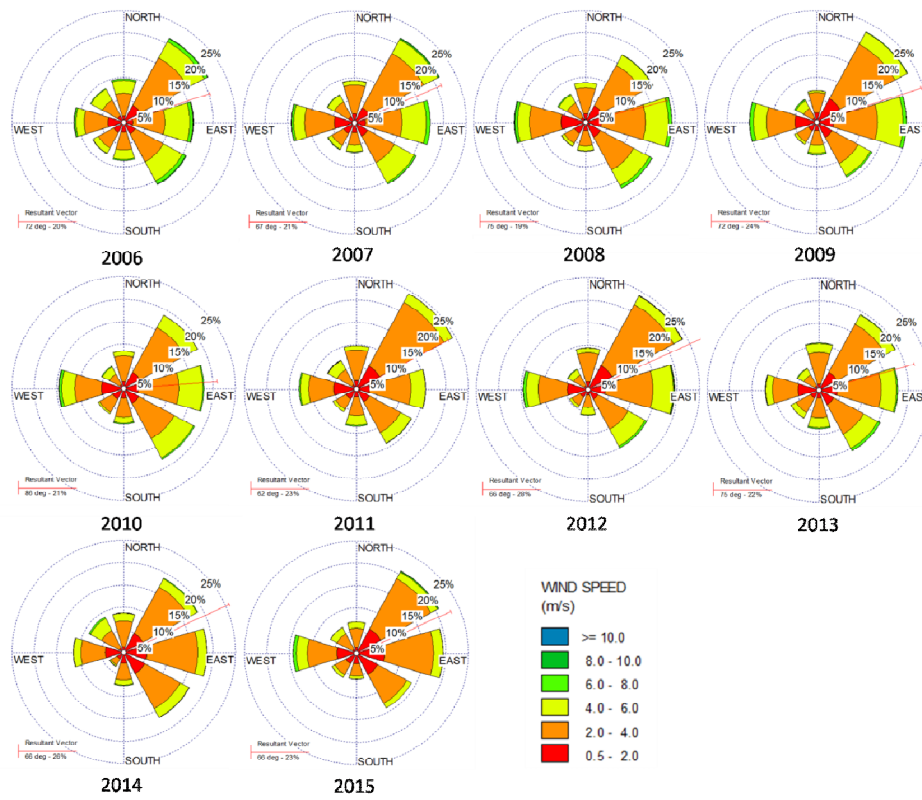
1039





1040  
 1041  
 1042  
 1043  
 1044  
 1045  
 1046

**Figure 4.** The annual variation of (a) summer wind speed ( $\text{m s}^{-1}$ ) and (b) total solar radiation ( $\text{W m}^{-2}$ ) from 2006 to 2015 in Shanghai. Both wind speed and the solar radiation present weak inter-annual variations but without significant trends.



1047

1048

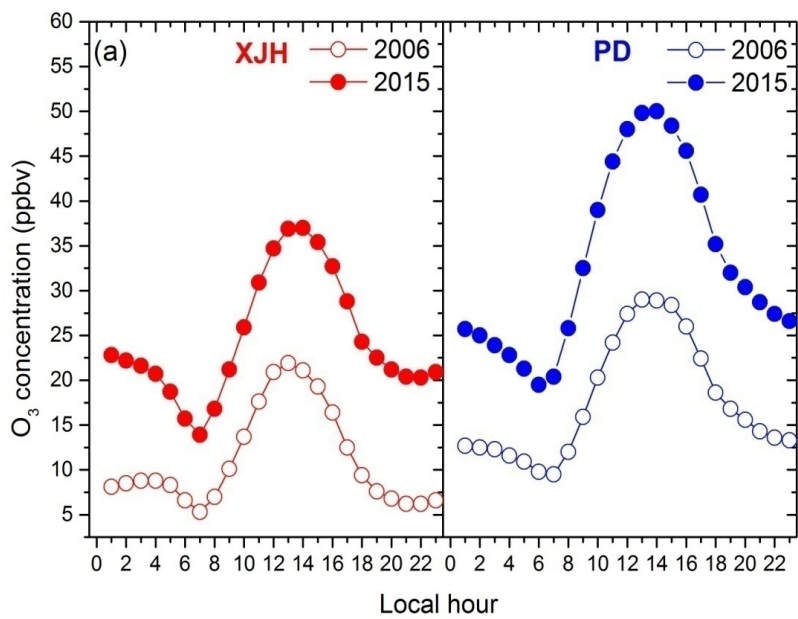
**Figure 5.** The wind rose of each year from 2006 to 2015 in Shanghai. The red line means the resultant vector suggesting the dominant wind direction.

1049

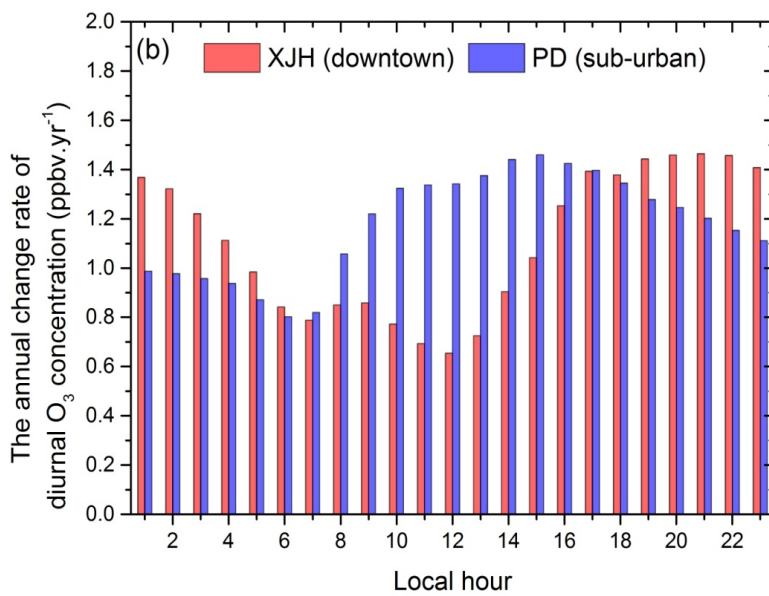
1050

1051

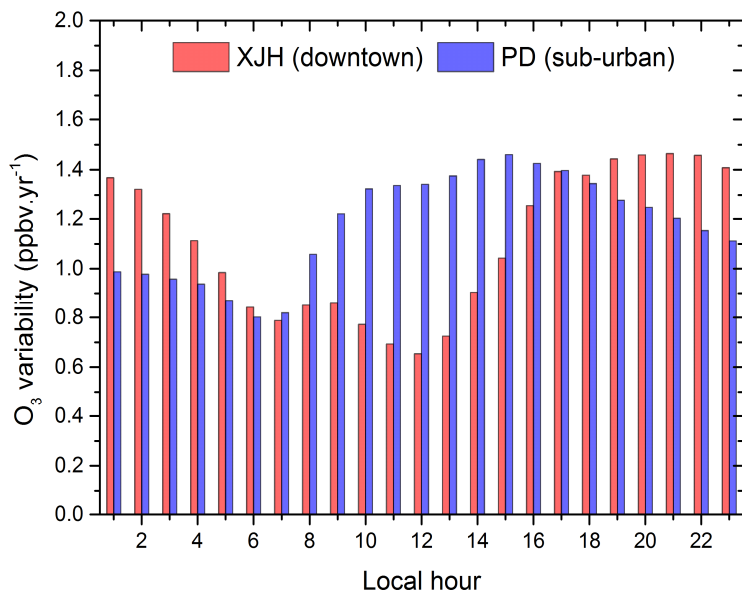
1052



1053



1054

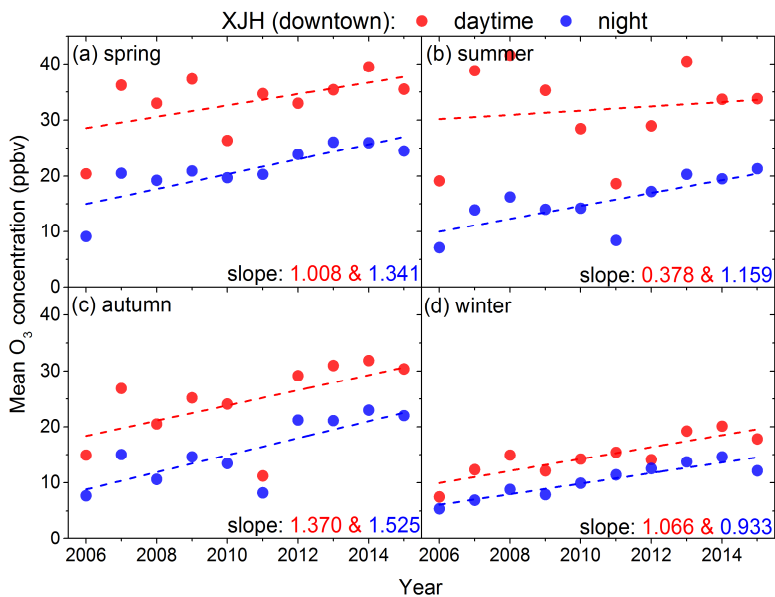


1055

1056 **Figure 6.** (a) The mean diurnal variation of  $O_3$  concentration (ppbv) compared between 2006 and  
 1057 2015 in XJH (red dots) and PD (blue dots). (b) The annual variability change rate of hourly diurnal  
 1058  $O_3$  concentration ( $ppbv.yr^{-1}$ ) from 2006 to 2015 at downtown site XJH (red bars) and sub-urban  
 1059 site PD (blue bars).  
 1060

带格式的：下标

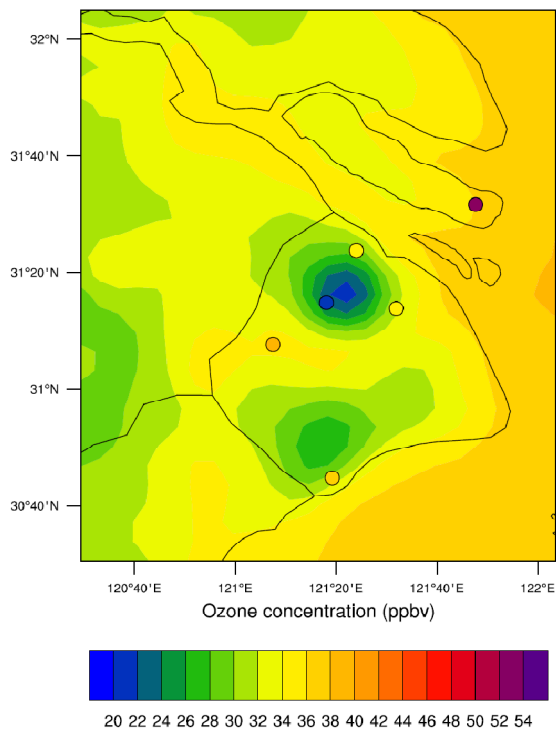
带格式的：上标



1061

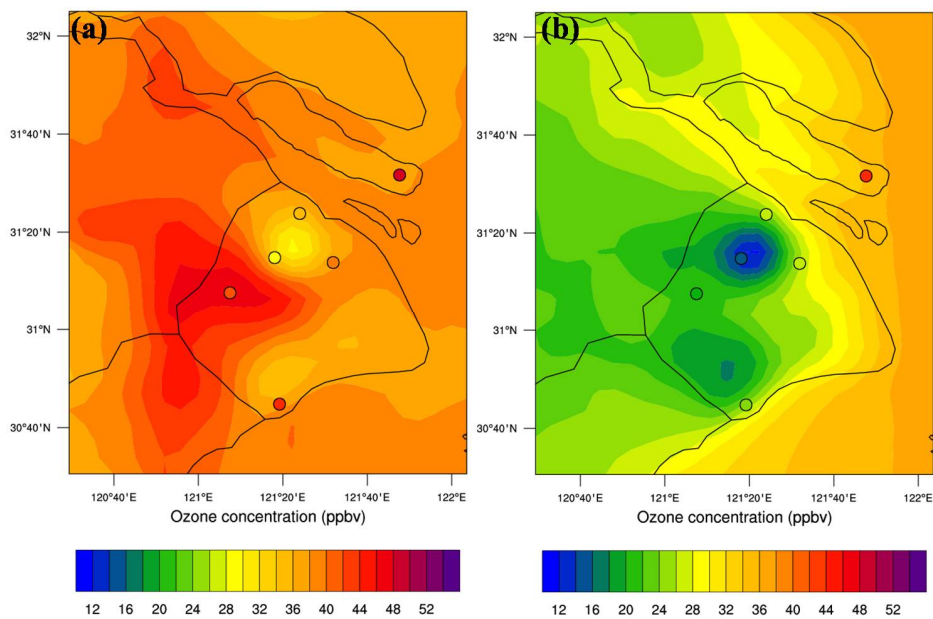
1062 **Figure 7.** The daytime (8:00-18:00, BJT) and nighttime (19:00-07:00, BJT)  $O_3$  variability from 2006  
 1063 to 2015 at downtown site XJH in (a) spring, (b) summer, (c) autumn and (d) winter.  
 1064

1065



带格式的：左

1066

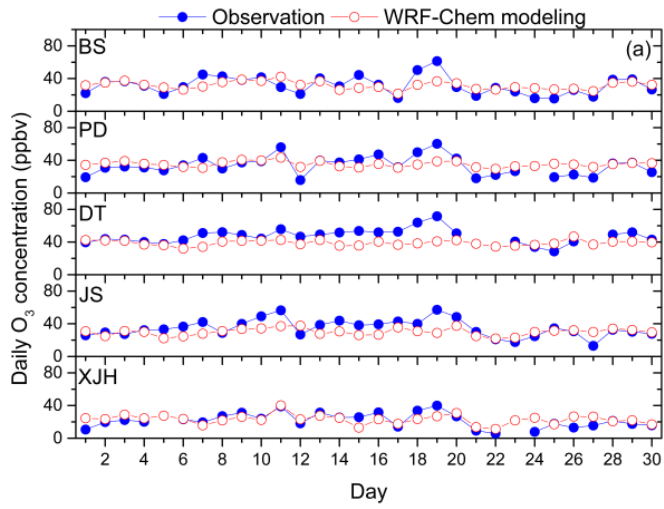


1067

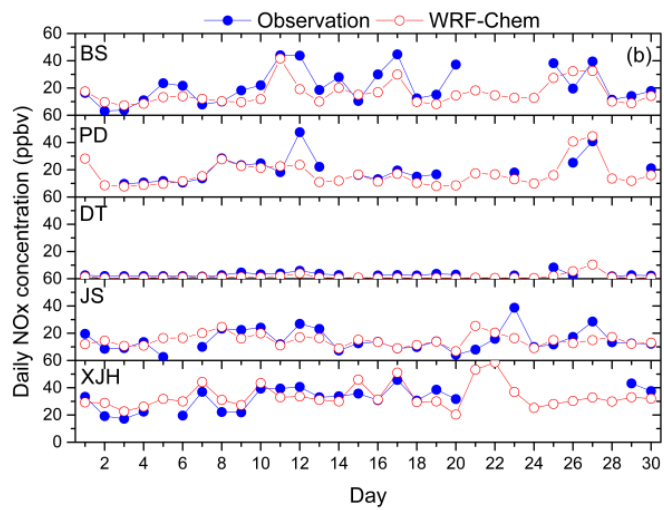
1068 **Figure 8.** The calculated distribution of (a) daytime and (b) nighttime  $O_3$  concentration by  
1069 WRF-Chem (shade) in September of 2009 compared with measurements (circles) of 6 sites over  
1070 Shanghai. The minimum  $O_3$  concentrations in daytime and nighttime both occur in urban center.

带格式的：下标

1071



1072



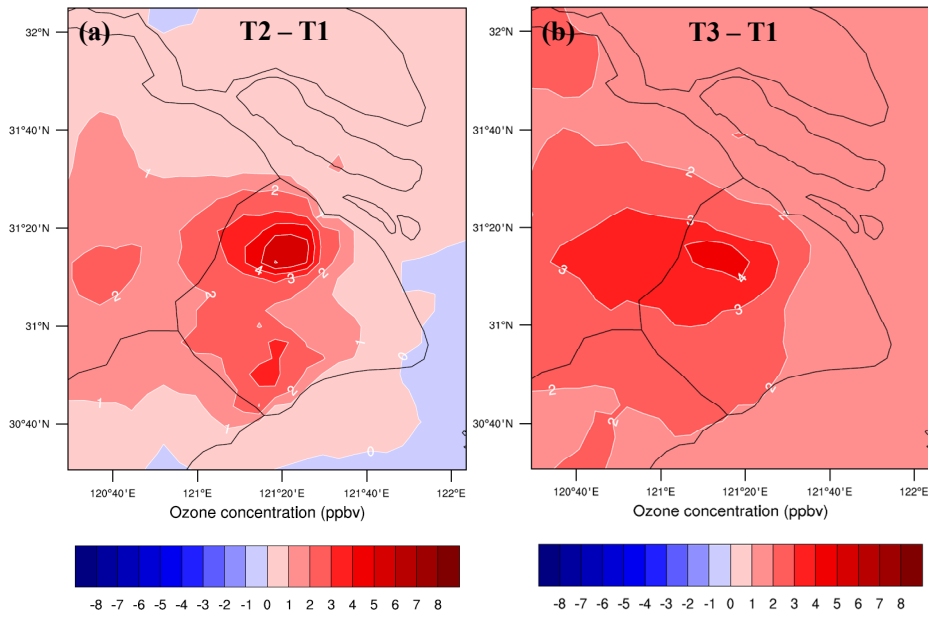
1073

1074

**Figure 9.** The calculated mean daily concentrations (ppbv) of (a)  $O_3$  and (b)  $NO_x$  at 5 sites in September of 2009 by WRF-Chem (red circles) and compared with measurements (blue circles).

1075

1076



1077

1078

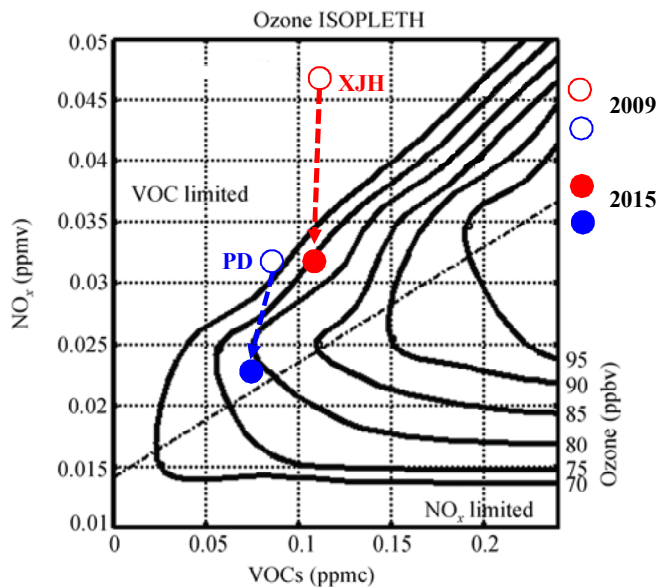
1079

1080

1081

1082

**Figure 10.** The difference of O<sub>3</sub> concentration (ppbv) between (a) T2 and T1 (T2-T1), (b) T3 and T1 (T3-T1) respectively conducted by WRF-Chem model. The difference between T2 and T1 lies in the NO<sub>x</sub> emissions set in T2 (2015 scenario) is 30% lower than that in T1 (2009 scenario), which is estimated by Lin et al. (2017) according to the Shanghai Environment Yearbook. The difference between T3 and T1 is dependent on that the VOCs emission in T3 is 50% higher than that in T1.



1083

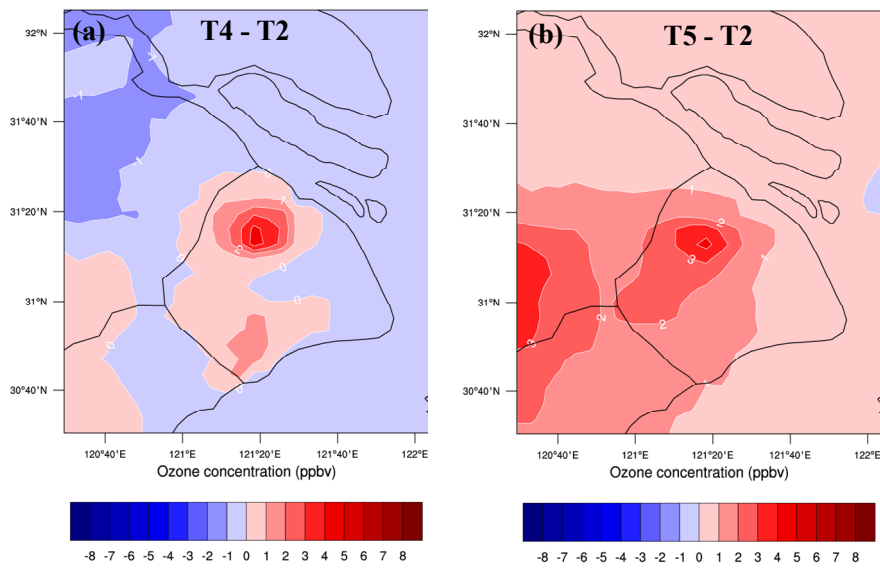
1084

1085

1086

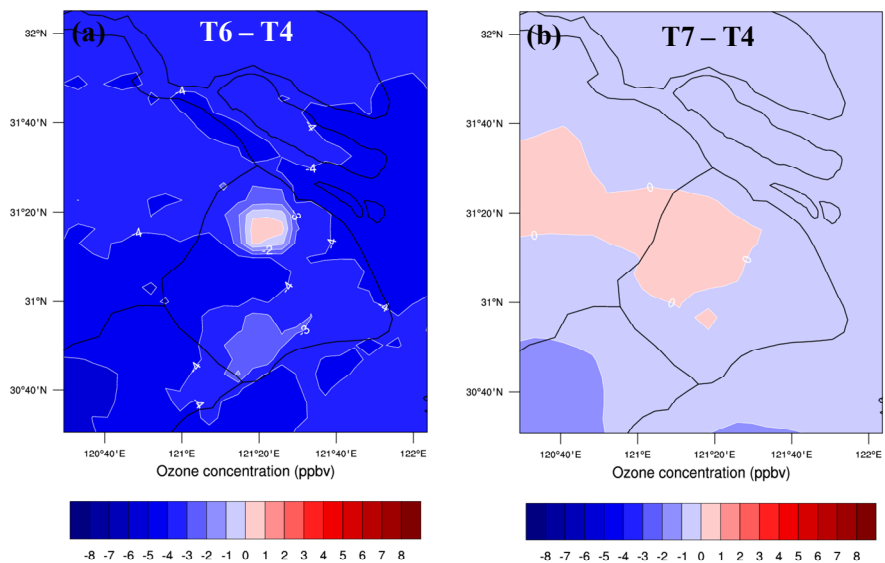
1087

**Figure 11.** The O<sub>3</sub> chemical production at downtown site XJH and sub-urban site PD in 2009 and 2015 depicted by O<sub>3</sub> isopleths diagram. The hollow and solid red circles denote O<sub>3</sub> production regime at XJH in 2009 and 2015 respectively. The hollow and solid blue circles denote O<sub>3</sub> production regime at PD in 2009 and 2015 respectively



1088  
 1089 **Figure 12.** The difference of O<sub>3</sub> concentration (ppbv) between (a) T4 and T2 (T4-T2), (b) T5 and  
 1090 T2 (T5-T2) respectively conducted by WRF-Chem model. The difference between T4 and T2 is  
 1091 that the NO<sub>x</sub> emissions set in T4 (2020 scenario) is 20% lower than that in T2 (2015 scenario),  
 1092 which is estimated according to the Shanghai Clean Air Action Plan. The difference between T5  
 1093 and T2 lies in that the VOCs emission in T5 is 50% higher than that in T2.  
 1094  
 1095  
 1096  
 1097





1098  
 1099 **Figure 13.** The difference of O<sub>3</sub> concentration (ppbv) between (a) T6 and T4 (T6-T4), (b) T7 and  
 1100 T4 (T7-T4) respectively conducted by WRF-Chem model. The NO<sub>x</sub> emissions set in T6 is 20% lower  
 1101 than that in T4 (2020 scenario). The VOCs emission in T7 is 50% higher than that in T4.